

Aggregated Author Response Document

We thank Editor Donahue for the opportunity to further refine and improve the manuscript.

In summary, we have:

- made several modifications to clarify the limitations of the current study,
- provided additional description of the oxidation pathways relevant for PMO-2, and
- improved the overall readability of the manuscript.

Overall despite the study limitations, the observations reported here have important implications for atmospheric aging and transport of organic aerosol in the free troposphere. We believe our unique sample set and detailed molecular analytical approach provides a unique opportunity to consider the implications on aerosol aging associated with respect to the transport pathways, meteorological conditions, and aerosol phase state.

A point-by-point response to each of the reviewer comments and a tracked changes version of the manuscript are provided below.

Author Responses to Reviewer #1

We thank Reviewer #1, Alexander Vogel, for his evaluation of the revised ACPD manuscript and useful comments, which helped us further improve the manuscript. The referee agrees that this paper provides a novel approach for assessing the aging of aerosol with highly relevant atmospheric implications, and that it should be published after including a more critical discussion on aerosol composition and processing.

In this reply *the Reviewer comments are given in black italic font* and *the Authors responses are given in blue font*. Manuscript text that we added or revised to address the comments is given in **bold font**. All page and line numbers are for the final revised manuscript (note, the line numbers in the tracked changes version of the manuscript are different due to inline tracking).

The revised manuscript „Molecular and physical characteristics of aerosol at a remote marine free troposphere site: Implications for atmospheric aging“ by Schum et al. has improved compared to the initial submission. The authors immediately corrected the misassigned back-trajectory analysis in Fig.1. They evaluated the possible bias in calculating the glass transition temperature by small weight molecules, which are lost during sample preparation. The authors show that small weight molecules, such as oxalic acid, only marginally influence the overall glass transition temperature. However, other small organic acids (acetic acid, formic acid) do have a pronounced influence on the glass transition temperature.

One main point noticed in the earlier discussion was that the authors discuss the differences of DI-ESI-signatures of samples with different emission sources, and conclude that the conditions during transport to PMO are the cause of the different chemical signature. The authors have addressed this point by acknowledging that the emission sources on their own do play a role (l. 504). However, in my opinion, the authors still do not adequately discuss this aspect throughout their current manuscript (except the parenthesis in l. 504). What is still missing is a discussion on possible secondary gas phase processes in an anthropogenic pollution plume (sample PMO-2), in which high NO_x, high SO₂, and secondary ozone can also result in completely different conditions, compared to the biomass burning plumes (PMO-1 and 3).

To address the reviewer's concern that we did not sufficiently clarify the significance of different emission sources, we added/revised the following text:

- Lines 308-314: **“The North American boundary layer outflow of organic aerosol captured in PMO-2 was likely influenced by SOA (Zhang et al., 2007) and thus is expected to have a higher**

initial O/C value compared to pyro-convected wildfire emissions of organic aerosol (e.g., Aiken et al., 2008; Jimenez et al., 2009; Bougiatioti et al., 2014). Although the initial compositions are unknown, we anticipated that the samples with longer transport times (~ 1 week for PMO-1 and PMO-3) would be at least similar or perhaps more oxidized than PMO-2 which had a much shorter transport time (~ 3 days). This expectation was based on literature describing secondary organic aerosol formation and aging (Volkamer et al., 2006; Jimenez et al., 2009) and the reported molecular composition of continental boundary layer aerosol (Mazzoleni et al., 2012; Huang et al., 2014).”

- Lines 366-370: “The increased number of sulfur species observed in PMO-2 is likely associated with the anthropogenic emission sources in the North American boundary layer. Overall, the observed differences in the O/C ratios between the boundary layer transported aerosol (PMO-2) compared to the free troposphere transported aerosol (PMO-1 and PMO-3) highlight differences in the aging and lifetime of aerosol relative to its transport pathway and emission source.”
- Lines 516-517: “PMO-2 aerosol were transported primarily through the boundary layer over the Northeast continental U.S. and the North Atlantic Ocean and was largely influenced by anthropogenic and biogenic sources.”

To address the reviewer’s concern that we did not sufficiently discuss the secondary gas phase processes, we added the following text:

- Lines 486-492: “However, the exact oxidation pathways that led to the increased oxidation observed for PMO-2 and its initial composition are unclear. Both gas phase and aqueous phase reactions lead to SOA formation, where aqueous SOA components can have higher O/C values than gas phase SOA components (Lim et al., 2010; Ervens et al., 2011). The high numbers of CHNO and CHOS molecular formulas observed here are consistent with secondary components associated with an emission plume likely enriched in SO₂, NO_x, and O₃ pertaining to its expected anthropogenic influence. All three of these reactive species have been shown to lead to production and oxidation of SOA in the atmosphere (Hoyle et al., 2016; Bertrand et al., 2018).”
- Lines 506-509: “While clearly gas phase SOA cannot be excluded, several lines of evidence suggest that aqueous phase oxidation likely influenced the chemical and physical characteristics of the PMO-2 aerosol to a larger extent than those of PMO-1 and PMO-3 based on the observed molecular characteristics, major ion concentrations (Fig. S20), and the model simulated transport pathways and GFS meteorology.”

In their response to the reviewer’s comments, the authors argue that aqueous phase processing “leads to SOA production with a greater array of carbon numbers; the greater number of carbon numbers matches more closely with our observations of a continuum of carbon numbers from 2 to 33 in PMO-2”. This argument does not seem convincingly to me, since there is a clear continuum of carbon numbers in the same range for PMO-1 and PMO-3 (Fig. 4 (a)-(c)), as well. The continuum of carbon numbers is actually the largest in PMO-1 (the biomass burning sample), resulting in ion signals up to 700 amu (Fig. 2 (a)). Thus, it looks like the emission source rather dominates the observed carbon number array.

The reviewer appears to have misunderstood our comment in the previous response document.

The original response in Author Responses to Reviewer #1 (last paragraph on page 2) was “Auto-oxidation as described by Crounse et al. (2013), Ehn et al. (2012), and Jokinen et al. (2014) does increase the O/C, but it also shows clear carbon number preferences associated with the oxidation of terpene precursors. This trend is consistent with our earlier work on condensed SOA where the concept of “auto-oxidation” was described as “oxygen-increasing-reactions” (Kundu et al., 2012). However, in the case of PMO-2, we did not observe carbon number preferences, which would indicate auto-oxidation. While this does not negate the possible influence of auto-oxidation, it does minimize its relative importance for these long range transported aerosol observations. On the other hand, aqueous phase processing as described by Lim et al. (2010) leads to SOA production with a greater array of carbon numbers; the greater array of carbon numbers matches more closely with our observations of a continuum of carbon numbers from 2 to 33 in PMO-2. “

Thus, the phrase “a greater array of carbon numbers” specifically referred to the dispersion of ion intensity over the range of carbon numbers for aqueous phase SOA vs. auto-oxidation. It by no means compares the range of carbon values for emission sources. The well-known polymeric signatures at specific carbon numbers is routinely observed with terpene SOA, but not aqueous SOA and not combustion emissions. Therefore, a continuum of carbon numbers does not imply an emission source.

I like the idea of comparing the PMO samples with samples of cloud and fog water (Table S.6) to identify compounds that are unique markers for aqueous phase processing. While the comparison between Cook et al. (2017) and PMO shows in fact the largest number of signals in common with PMO-2, the comparison with Zhao et al. (2015) shows the majority of common signals with PMO-1. We see that O/C of the comparison is highest for the sample PMO-2, but it remains unclear whether this is driven by the stronger presence of high O/C compounds in PMO2, which are not present in the samples PMO1/3. Thus, to me it remains elusive that this comparison is a clear indication for the “influence of aqueous phase processing” in sample PMO2.

This line of evidence, in conjunction with the other lines of evidence that we have put forward (back trajectories, RH, and ion concentrations), supports our hypothesis for the influence of aqueous processing on the observed oxidation of PMO-2. Furthermore, Figure S19 shows the species that are uniquely common between each of the PMO samples and the SPL cloud water. In it, the formulas in PMO-2 are clearly focused in the more oxidized region of the plot, while the majority of the unique formulas for PMO-1 and PMO-3 are in less oxidized, lower O/C regions of the plot. The rest of the formulas are common between two or more of the samples are thus fairly well accounted for when calculated the average O/C. In other words, the greatly increased O/C observed for the species common between PMO-2 and the cloud water is driven by the presence of high O/C formulas that are not present in the other samples.

Note we assumed the reviewer intended to refer to Zhao et al. (2013), as we've previously cited, instead of (2015).

Concerning ESI-artifacts: I do believe that negative ESI is less prone to adduct artifacts than positive ESI. The authors mentioned that samples are diluted to the lowest possible level to obtain a stable current during ESI. In principle, ESI should form always a stable current- even without any analyte present (e.g. in blank measurements). The authors mention that their AGC target of 1e6 ions was reached after 20-80 ms. I compared this to injection times on a Q-Exactive System (AGC target 1e6) after chromatographic separation – same ballpark. Thus, it seems that the samples were in fact reasonably diluted, however, it would also be interesting to see the actual ion count rates. I am asking for these numbers, since the NL value of the MS/MS experiments seem to me rather low (e.g. 5e3 for m/z 300 +/- 3). Such low value can be an indication for the presence of cluster ions, provided that the ion signal in the full scan shows a much higher signal (not possible to evaluate here, since the numbers are not reported).

The normalization levels (NL) shown in the mass spectra are arbitrary values corresponding to the ion intensity of the base peak and not the total number of ions (corresponding to the auto-gain control (AGC) setting). The NL levels on the FT-ICR MS (FT Ultra, Thermo Scientific) are a few orders of magnitude lower than they are in the Orbitrap MS (e.g., Orbitrap Elite, Thermo Scientific). The FT-ICR MS instruments are significantly less sensitive than the Orbitrap MS instruments; thus, co-addition of 200 recorded transient spectra is routinely done with FT-ICR MS (as described in lines 180-182). We have observed NL values of $10^3 - 10^5$ on the FT-ICR MS and NL values of $10^7 - 10^8$ on the Orbitrap Elite. We do not know how either of these instruments compare to the Q-Exactive System.

The mass spectra we studied do not show evidence of ESI artifacts. We believe this is because we analyze dilute solutions using negative ion ESI after reverse phase SPE isolation to remove the inorganic salts and low molecular weight organic salts that are possible adducting species (e.g., lines 158-164). Further analysis of the MS/MS spectra is beyond the scope of the current manuscript.

Overall, I see the strength of this paper in relating the extracted conditions (T and RH) during transport with the observed chemical composition. But, I do miss a solid chain of reasoning toward the hypothesis of aqueous-phase aging in the MBL in contrast to slow aging rates in the FT when the aerosol is in a glassy state. It all goes back to the fact that the samples have a completely different source (anthropogenic pollution vs biomass burning), and the chemical signature of the aerosol, when it is close to its emission source (t_{zero} of aging), is not known. Thus, I do not see point 5 of the ACP review criteria fulfilled (Are the results sufficient to support the interpretations and conclusions?). Still, the paper provides a novel and interesting concept: the extraction of glass transition temperatures from molecular ion measurements. Also the atmospheric implications are highly relevant: slow aging rates of BB aerosol and slow decomposition of BrC in the free troposphere. Therefore, I recommend the article to be published in ACP after a more critical discussion regarding the fact that the initial aerosol composition in plume PMO2 (when it is still over the continent) is not known, and that other processes in the plume than only aqueous-phase oxidation during transport could explain the high O/C of the sample PMO-2.

We thank the reviewer for highlighting the strengths of the manuscript and the recommendation to be published in ACP. To address the reviewer's concern regarding the need for additional discussion on the initial aerosol composition and other potentially present processes, we additionally revised the following paragraph (lines 484-509) describing the oxidation of PMO-2. Here we include the entire paragraph with all changes in bold, although some of the sentences from this paragraph were already mentioned above.

"As described above, the most obvious difference in the molecular composition of PMO-2 vs. PMO-1 and PMO-3 is the increased extent of oxidation. In fact, most of the unique species observed in PMO-2 are in the highly oxidized region of the van Krevelen plot (Fig. 8). However, the exact oxidation pathways that led to the increased oxidation observed for PMO-2 and its initial composition are unclear. Both gas phase and aqueous phase reactions lead to SOA formation, where aqueous SOA components can have higher O/C values than gas phase SOA components (Lim et al., 2010; Ervens et al., 2011). The high numbers of CHNO and CHOS molecular formulas observed here are consistent with secondary components associated with an emission plume likely enriched in SO₂, NO_x, and O₃ pertaining to its expected anthropogenic influence. All three of these reactive species have been shown to lead to the production and oxidation of SOA in the atmosphere (Hoyle et al., 2016; Bertrand et al., 2018). Cloud and aqueous phase processing have also been shown to increase the oxidation of atmospheric organic matter (e.g., Ervens et al., 2008; Zhao et al., 2013; Cook et al., 2017; Brege et al., 2018). Comparisons of the detailed molecular composition of the PMO samples with studies of cloud (Zhao et al., 2013; Cook et al., 2017) and fog (Mazzoleni et al., 2010) organic matter indicate that the formulas uniquely common to only PMO-2 have higher O/C, which supports aqueous phase processing during transport. These results are provided in Fig. S19 and Table S6. Studies have shown that the reactive species emitted from anthropogenic plumes (SO₂, NO_x, O₃) can play a role in the oxidation of the

organic species that are dissolved in water (Blando and Turpin, 2000; Chen et al., 2008; Ervens et al., 2011). Furthermore, studies have shown that aerosol liquid water content contributes to aqueous production of SOA (Volkamer et al., 2009; Lim et al., 2010). The elevated RH extracted from the GFS for this plume (Fig. 7) indicates the presence of aerosol liquid water and is consistent with its ubiquitous nature (Nguyen et al., 2016). Additionally, PMO-2 had a strongly elevated non-sea salt sulfate concentration relative to PMO-1 and PMO-3, which also indicates aqueous phase processing (Crahan et al., 2004; Yu et al., 2005; Sorooshian et al., 2007; Hoyle et al., 2016). Oxalate, another well-known marker of aqueous phase processing (Warneck 2003; Crahan et al., 2004; Yu et al., 2005; Sorooshian et al., 2007; Carlton et al., 2007), was also elevated in PMO-2. The organic mass fraction of oxalate was 9.4 % in PMO-2 compared to 2.3 % and 3.0 % in PMO-1 and PMO-3. The nitrate concentration in PMO-2 was very low compared to PMO-1 or PMO-3 (Table 1), also supporting aqueous phase processed aerosol in PMO-2. While clearly gas phase formation of SOA cannot be excluded, several lines of evidence suggest that aqueous phase oxidation likely influenced the chemical and physical characteristics of the PMO-2 aerosol to a larger extent than those of PMO-1 and PMO-3 based on the observed molecular characteristics, major ion concentrations (Fig. S20), and the model simulated transport pathways and GFS meteorology.”

We modified the abstract to note directly that we have a limited number of observations (lines 21-23): “**Although the number of observations is limited**, the results suggest that biomass burning organic aerosol injected into the free troposphere are more persistent than **organic aerosol** in the boundary layer having broader implications for aerosol aging.”

The following changes were also applied to clarify the potential effect of emission sources:

- Lines 120-121: “We observed key molecular differences **pertaining to the extent of oxidation** likely related to the **combination of** transport pathways and their apparent emission sources.”
- Lines 308-312: “**The North American boundary layer outflow of organic aerosol captured in PMO-2 was likely influenced by SOA (Zhang et al., 2007)** and thus is expected to have a higher initial O/C value compared to **pyro-convected** wildfire emissions of organic aerosol (e.g., Aiken et al., 2008; Jimenez et al., 2009; Bougiatioti et al., 2014). **Although the initial compositions are unknown**, we anticipated that the samples with longer transport times (~ 1 week for PMO-1 and PMO-3) would be **at least similar or perhaps** more oxidized than PMO-2 which had a **much** shorter transport time (~ 3 days).”
- Lines 366-368: “**The increased number of sulfur species observed in PMO-2 is likely associated with the anthropogenic emission sources in the North American boundary layer.**”

Specific comments:

l. 13-16: Here the authors conclude that “environmental factors during transport” are responsible for the higher O/C in PMO-2. I am missing any mentioning of the possibility of different chemical composition (e.g. already higher O/C) of the PMO2 plume right at its source. Also, the term “environmental factors during transport” is too blurry.

To clarify this, the sentence was replaced with the following: “**To better understand the difference between free tropospheric transport and boundary layer transport, the meteorological conditions along the FLEXPART simulated transport pathways were extracted from the Global Forecast System analysis for model grids.**” (Lines 15-17)

l. 20: The same issue here: the comparison between PMO1/3 and PMO2 has to be discussed with more caution. The data presented do not allow the conclusion that solely Tg/T is the cause of higher oxidized

aerosol in PMO2. I recommend something like “[...] and therefore less susceptible to oxidative aging than the organic aerosol transported in the boundary layer.”

We agree that PMO-1 and PMO-3 are less susceptible to oxidative aging and thank the reviewer for his suggestion of how to clarify the text. We changed the mentioned sentence which now reads (lines 19-21): “Comparisons of the T_g to the ambient temperature indicated that a majority of the organic aerosol components transported in the free troposphere were more viscous and therefore **less susceptible to oxidation** than the organic aerosol components transported in the boundary layer.”

l. 28: [...] cloud droplet and ice nucleation activity [...]?

We added the word “**activity**” to mentioned sentence and its beginning now reads (lines 28-29): “Oxidation of organic aerosol impacts its lifetime, cloud droplet and ice nucleation **activity**, ...”

l. 34-36: The biomass burning studies cited here might not be the best, since they all refer to biomass burning events from gassland fires. Grass-lignin is different from softwood (coniferous) lignin, resulting in different biomass burning marker molecules (Simoneit et al., 1993). Referring to studies on biomass burning plumes from boreal forest fires (e.g. Corrigan et al. (2013)) might be more appropriate in the context of discussing plumes from Canadian boreal forests. It is well recognized that the most prominent organic biomass burning marker (levoglucosan) undergoes fast photooxidation, however, I did not find a connection between biomass burning markers and their oxidative degradation in the paper by Vakkari et al., 2014. Here, a paper on the degradation kinetics of levoglucosan would fit much better (e.g. Lai et al. (2014), Arangio et al. (2015))

The references illustrate that rapid oxidation occurs in both anthropogenic and biomass burning aerosol within the boundary layer. Corrigan et al., 2013 is consistent with these, so we added it (lines 35-37): “Rapid oxidation was also observed in studies of biomass burning organic aerosol in Africa (Capes et al., 2008; Vakkari et al., 2014), over the Mediterranean Sea (Bougiatioti et al., 2014), and **Hyytiälä, Finland** (Corrigan et al., 2013; Vogel et al., 2013).”

To clarify the rapid oxidation of levoglucosan the following sentence was added (lines 37-40): “**Other studies focused on the oxidation of molecular tracers such as levoglucosan have shown that they can be degraded rapidly after emission, depending on the atmospheric conditions (Lai et al., 2014; Slade et al., 2014; Arrangio et al., 2015; Bertrand et al., 2018). These studies all demonstrate** the importance of oxidation to the aging of organic aerosol and provide motivation for studies of long-range transported organic aerosol.”

l. 38: The authors might find our paper on long-range-(low-altitude)-transported biomass burning aerosol from wildfires in Russia to the SMEAR station in Hyytiälä, Finland of interest. During a pollution plume event we observed highly oxidized aerosol ($O/C \sim 0.70$), while the average O/C during this campaign ranged around 0.5. We also observed high-molecular weight organic matter in the aerosol phase during this BB event, indicated by molecular ion signals up to m/z 800 (Vogel et al., 2013).

We thank the reviewer for pointing out this interesting paper, which is highly relevant for this work.

l. 244: A low oxalate/sulfate ratio is reported for PMO-2, likely obscured by high sulfate concentrations. The authors argue that oxalate is also high in PMO-2 due to aqueous phase processing. To further search for evidence that cloud processing has really occurred for PMO-2, it would be of interest to compare the oxalate/sulfate ratio in sample PMO2 with reported oxalate/sulfate ratios in the Eastern US close to the emission sources.

It was difficult to obtain oxalate/sulfate ratios for fresh aerosol in the Eastern US, but we did find some ratios for aerosol from Helsinki, Southern Africa, Hong Kong, and the Amazon (Zhou et al., 2015). The ratios from PMO-2 compared to the non-BB ratios from Zhou et al. noticeably exceed those reported for Helsinki, Southern Africa, and Hong Kong (Note, only BB aerosol values were reported for the Amazon sample). Based on the studies by Yu et al., (2005) and Sorooshian et al., (2007) the observed oxalate/sulfate ratio further supports our hypothesis of aqueous processing for this sample.

l. 307: Is the North American SOA solely anthropogenic? I think there are several studies reporting dominant biogenic SOA in East America (e.g. isoprene SOA in South East US?).

We thank the reviewer this comment and agree with the reviewer it is likely that biogenic SOA are a significant component of the aerosol. As stated above, to make this more clear we added the following text (lines 308-310): “**The North American boundary layer** outflow of organic aerosol **captured in PMO-2 was likely influenced by SOA (Zhang et al., 2007) and thus** is expected to have a higher **initial O/C** value compared to **pyro-convected** wildfire emissions of organic aerosol (e.g., Aiken et al., 2008; Jimenez et al., 2009; Bougiatioti et al., 2014).”

l. 353-366: The authors describe a higher O/C in PMO2 for the CHOS group compared to PMO1, and argue at the end of the section that this observation highlights the enhanced aging during transport of PMO2. While I believe that there is indeed a higher oxygen content in the sample PMO2, it does matter to which atom the oxygen is bonded. If it appears as oxygen-sulfur bonds (as organosulfates), then the increased oxygen content (higher O/C) in PMO-2 rather tells us that the different source emissions of the PMO2 plume allowed enhanced formation of organosulfates. This observation would be in line with the observation of higher inorganic sulfate in PMO2, as well as the expectation that SO2 emissions over North East US are higher than in the remote Canadian boreal forests.

Yes, because of the ESI analytical bias the sulfur containing formulas in our samples are likely organosulfates. We also carried this assumption through the calculation of the average oxidation state of carbon as stated in lines 374-375: “Additionally, we assumed all nitrogen and sulfur were present as nitrate and sulfate functional groups and calculated the O_{Sc} with the appropriate corrections (Equation S1).”

The presence of organosulfates indicates that reactive sulfur was present, which we described as being due in part to anthropogenic emissions (line 246). To strengthen the connection between the CHOS formulas and the emission source we added the following text (lines 366-370): “**The increased number of sulfur species observed in PMO-2 are likely associated with the anthropogenic emission sources in the North American boundary layer.** Overall, **the observed** differences in the O/C ratios between the boundary layer transported aerosol (PMO-2) compared to the free troposphere transported aerosol (PMO-1 and PMO-3) highlight differences in the aging and lifetime of aerosol relative to its transport pathway **and emission source.**”

Regarding an artificially increased O/C value, we repeat our original response to this concern in Author Responses to Reviewer #1 (second paragraph on page 16): “Yes, the O/C of the CHOS species is impacted by the presence of organic sulfates. If 4 oxygen (atoms) are removed from the molecular formulas and the O/C is recalculated the O/C decreases to a level somewhat below that of the CHO group (O/C = 0.44 for PMO-2 and O/C = 0.27 for PMO-1 when “sulfate” is removed). This is why the O/C values of the CHOS compounds are not directly compared to the other (elemental) groups.”

l. 380: It is too speculative to talk about the CCN ability of the sampled aerosol particles when their size distribution is not known. Also, the speculation about the amount of less volatile components seems to me

ambiguous, since the total mass concentration available for gas-to-particle partitioning will also affect the fraction of higher-volatility compounds in the particle phase.

We did not intend to imply that we knew the CCN ability of the sampled aerosol, only that based on the observed characteristics the aerosol would have a higher CCN ability. Likewise, the most abundant components were less volatile in PMO-2, as demonstrated by the volatility plots (Figs. 6, S13, S14). To make this more clear, we have made the following changes to the sentence: “Conversely, the overall higher oxidation of PMO-2 implies that the sampled aerosol was likely more hygroscopic, included more efficient cloud condensation nuclei (Massoli et al., 2010), **or had components of a less volatile nature** (Ng et al., 2011) **than PMO-1 and PMO-3.**” (Lines 383-385)

+l. 472: What is about the role of multiphase and heterogeneous oxidation of the aerosol additionally to aqueous-phase processing of cloud droplets?

In this case, we referred to oxidation processes in general and only exemplify aqueous phase oxidation because the predicted RH during transport varied strongly between the boundary layer and the free troposphere. This implies that aqueous-phase oxidation/processing would be especially limited in the free troposphere. Note, we do not have trace gas concentrations and thus we chose to avoid speculation regarding the gas-phase oxidation process differences. As such, we decided to leave this sentence as is.

l. 480-494: The section is missing a more critical discussion, including the fact that the initial chemical composition of the plume sampled in PMO2 is not known. Again, PMO2 is compared here against PMO1 and 3. The fact that higher sulfate is observed in PMO2 compared with PMO1/3 rather goes back to the emission source, where you expect more SO2 being emitted in North America than in the boreal forest. The relatively higher abundance of sulfate in PMO2 against PMO1/3 hence does not necessarily support cloud processing.

To directly address the reviewers concern about not knowing the initial composition, we added the following: “**However, the exact oxidation pathways that led to the increased oxidation observed for PMO-2 and the initial composition are unclear.**” (Lines 486-487).

As for the reviewer’s concern about sulfate in PMO-2 vs. PMO-1/3, we mentioned several times that the sulfate concentration is related to the emission source. Manuscript text in lines 234-235, 246, 285, and 308-310 all makes direct or oblique mention of the impact of anthropogenic emissions on the concentration of sulfate or the observed oxidation. Additionally, as many studies have noted (Crahan et al., 2004; Carlton et al., 2007; Zhou et al., 2015), the production of sulfate is strongly tied to aqueous and cloud phase processing of SO₂ including when the emission source of SO₂ is anthropogenic.

In any case (and as described above), we have made several minor changes to this section to better address the concerns about initial composition and gas phase reactions.

l. 488-491: These lines are redundant with section 3.1 (l.235 ff.).

We removed the following sentence: “Furthermore, nitrate is known to be scavenged during cloud processing (Dunlea et al., 2009), leading to its decrease in recently cloud processed aerosol.”

l. 508: Only aqueous-phase oxidation?

No, it should be all oxidation, the sentence has been changed accordingly (Line 526).

References

Arangio, A. M., Slade, J. H., Berkemeier, T., Pöschl, U., Knopf, D. A., and Shiraiwa, M.: Multiphase chemical kinetics of OH radical uptake by molecular organic markers of biomass burning aerosols: humidity and temperature dependence, surface reaction, and bulk diffusion, *J. Phys. Chem. A*, 119, 4533–4544, doi:10.1021/jp510489z, 2015.

Corrigan, A. L., Russell, L. M., Takahama, S., Äijälä, M., Ehn, M., Junninen, H., Rinne, J., Petäjä, T., Kulmala, M., Vogel, A. L., Hoffmann, T., Ebbesen, C. J., Geiger, F. M., Chhabra, P., Seinfeld, J. H., Worsnop, D. R., Song, W., Auld, J., and Williams, J.: Biogenic and biomass burning organic aerosol in a boreal forest at Hytytälä, Finland, during HUMPPA-COPEC 2010, *Atmos. Chem. Phys.*, 13, 12233–12256, doi:10.5194/acp-13-12233-2013, 2013.

Lai, C., Liu, Y., Ma, J., Ma, Q., and He, H.: Degradation kinetics of levoglucosan initiated by hydroxyl radical under different environmental conditions, *Atmospheric Environment*, 91, 32–39, doi:10.1016/j.atmosenv.2014.03.054, 2014.

Simoneit, B.R.T., Rogge, W. F., Mazurek, M. A., Standley, L. J., and Hildemann, L.M., and Cass, G. R.: Lignin pyrolysis products, lignans, and resin acids as specific tracers of plant classes in emissions from biomass combustion, *Environmental Science & Technology*, 27, 2533–2541, 1993.

Vogel, A. L., Äijälä, M., Corrigan, A. L., Junninen, H., Ehn, M., Petäjä, T., Worsnop, D. R., Kulmala, M., Russell, L. M., Williams, J., and Hoffmann, T.: In situ submicron organic aerosol characterization at a boreal forest research station during HUMPPA-COPEC 2010 using soft and hard ionization mass spectrometry, *Atmos. Chem. Phys.*, 13, 10933–10950, doi:10.5194/acp-13-10933-2013, 2013.

References

Crounse, J. D., Nielsen, L. B., Jorgensen, S., Kjaergaard, H. G., and Wennberg, P. O.: Autoxidation of Organic Compounds in the Atmosphere, *Journal of Physical Chemistry Letters*, 4, 3513–3520, doi:10.1021/jz4019207, 2013.

Ehn, M., Kleist, E., Junninen, H., Petaja, T., Lonn, G., Schobesberger, S., Dal Maso, M., Trimborn, A., Kulmala, M., Worsnop, D. R., Wahner, A., Wildt, J., and Mentel, T. F.: Gas phase formation of extremely oxidized pinene reaction products in chamber and ambient air, *Atmos. Chem. Phys.*, 12, 5113–5127, doi:10.5194/acp-12-5113-2012, 2012.

Jokinen, T., Sipila, M., Richters, S., Kerminen, V.-M., Paasonen, P., Stratmann, F., Worsnop, D., Kulmala, M., Ehn, M., Herrmann, H., and Berndt, T.: Rapid Autoxidation Forms Highly Oxidized RO₂ Radicals in the Atmosphere, *Angewandte Chemie-International Edition*, 53, 14596–14600, doi:10.1002/anie.201408566, 2014.

Kundu, S., Fisseha, R., Putman, A. L., Rahn, T. A. and Mazzoleni, L. R.: High molecular weight SOA formation during limonene ozonolysis: insights from ultrahigh-resolution FT-ICR mass spectrometry characterization, *Atmos. Chem. Phys.*, 12(12), 5523–5536, doi:10.5194/acp-12-5523-2012, 2012.

Zhou, Y., Huang, X. H., Bian, Q., Griffith, S. M., Louie, P. K. K. and Yu, J. Z.: Sources and atmospheric processes impacting oxalate at a suburban coastal site in Hong Kong: Insights inferred from 1 year hourly measurements, *J. Geophys. Res-Atmos.*, 120(18), 9772–9788, doi:10.1002/2015jd023531, 2015.

Molecular and physical characteristics of aerosol at a remote-marine free troposphere site: Implications for atmospheric aging

Simeon K. Schum¹, Bo Zhang^{2,a}, Katja Dzepina^{1,b}, Paulo Fialho³, Claudio Mazzoleni^{2,4} and Lynn R. Mazzoleni^{1,2}

¹Department of Chemistry, Michigan Technological University, Houghton, MI, USA

²Atmospheric Sciences Program, Michigan Technological University, Houghton, MI, USA

³Institute for Volcanology and Risk Assessment – IVAR, University of the Azores, Angra do Heroísmo, Portugal

⁴Department of Physics, Michigan Technological University, Houghton, MI, USA

^anow at the National Institute of Aerospace, Hampton, VA, USA

^bnow at the Department of Biotechnology, University of Rijeka, Croatia

Correspondence to: Lynn R. Mazzoleni (lrmazzol@mtu.edu)

Abstract. Aerosol properties are transformed by atmospheric processes during long-range transport and play a key role in the Earth's radiative balance. To understand the molecular and physical characteristics of free tropospheric aerosol, we studied samples collected at the Pico Mountain Observatory in the North Atlantic. The observatory is located in the marine free troposphere at 2225 m above sea level, on Pico Island in the Azores archipelago. The site is ideal for the study of long-range transported free tropospheric aerosol with minimal local influence. Three aerosol samples with elevated organic carbon concentrations were selected for detailed analysis. FLEXPART retroplumes indicated that two of the samples were influenced by North American wildfire emissions transported in the free troposphere and one by North American outflow mainly transported within the marine boundary layer. ~~To determine the detailed molecular composition of the samples, we used ultrahigh~~ ^{Ultrahigh} resolution Fourier transform ion cyclotron resonance mass spectrometry ~~was used to determine the detailed molecular composition of the samples~~. Thousands of molecular formulas were assigned to each of the individual samples. On average ~60 % of the molecular formulas contained only carbon, hydrogen, and oxygen atoms (CHO), ~30 % contained nitrogen (CHNO), and ~10 % contained sulfur (CHOS). The molecular formula compositions of the two wildfire influenced aerosol samples transported mainly in the free troposphere had relatively low average O/C ratios (0.48 ± 0.13 and 0.45 ± 0.11) despite the 7 - 10 days of transport time according to FLEXPART. In contrast, the molecular composition of North American outflow transported mainly in the boundary layer had a higher average O/C ratio (0.57 ± 0.17) with 3 days of transport time. ~~Thus, aerosol oxidation appears to be related to environmental factors during~~ ^{To better understand the difference between free tropospheric} transport and ~~not simply aging time. We used~~ ^{boundary layer transport, the} meteorological conditions ~~along the~~ ^{along the} FLEXPART simulated transport pathways ~~were~~ extracted from the Global Forecast System analysis for ~~the~~ model grids ~~along the~~ ^{along the} FLEXPART simulated transport pathways. ~~We used the extracted meteorological conditions~~ and the observed molecular chemistry to predict the relative humidity dependent glass transition temperatures (T_g) of the aerosol components. Comparisons of the T_g to the ambient temperature~~,~~ indicated that a majority of the organic aerosol components transported in the free troposphere were more viscous and therefore less ~~oxidized~~ ^{susceptible to oxidation} than the organic aerosol components transported in the boundary layer. ~~This suggests~~ ^{Although the number of observations is limited, the results suggest} that biomass burning organic aerosol injected into the free troposphere are more persistent than ~~those~~ ^{organic} aerosol in the boundary layer having broader implications for aerosol aging.

1 Introduction

Atmospheric organic aerosol composition and mass concentrations are transformed by atmospheric processes including 30 oxidization (Dunlea et al., 2009; Jimenez et al., 2009; Kroll et al., 2011), cloud processing (Ervens et al., 2007, 2008, 2011; Zhao et al., 2013), and wet or dry deposition (Pöschl, 2005). Oxidation of organic aerosol impacts its lifetime, cloud droplet and ice nucleation activity (Massoli et al., 2010; Lambe et al., 2011; China et al., 2017), aerosol morphology, and optical properties (Pöschl, 2005; China et al., 2015; Laskin et al., 2015 and references therein). As such, the chemistry of atmospheric aerosol oxidation has received much attention (George and Abbatt, 2010; Lee et al., 2011; Kroll et al., 2011). Jimenez et al. 35 (2009) studied the oxidation of anthropogenic organic aerosol emitted from Mexico City as it was transported downwind. They used an aerosol mass spectrometer (AMS) instrument on board an aircraft to measure the magnitude of the *m/z* 44 fragment as a proxy for the oxidation of organic aerosol. After 6 hours and 63 km of transport, a noticeable increase in the overall chemical oxidation was observed. Rapid oxidation was also observed using an AMS in studies of biomass burning organic aerosol in Africa (Capes et al., 2008; Vakkari et al., 2014) and over the Mediterranean Sea (Bougiatioti et al., 2014). These analyses found that most of the marker species for biomass burning were oxidized within 24 hours (Vakkari et al., 2014) suggesting 40 that after 24 hours, organic aerosol is nearly indistinguishable regardless of source. Except for the study by Capes, and Hytylä, Finland (Corrigan et al., 2013; Vogel et al. (2008) the aerosol in these, 2013). Other studies was generally collected relatively close (up to 30 hours, but mostly < 10 hours downwind) to the focused on the oxidation of molecular tracers such as levoglucosan have shown that they can be degraded rapidly after emission sources, depending on the atmospheric conditions (Lai et al., 2014; Slade et al., 2014; Arrangio et al., 2015; Bertrand et al., 2018). These studies all show~~demonstrate~~ the 45 importance of oxidation to the aging of organic aerosol and provide motivation for studies of long-range transported organic aerosol.

A study of predominately Asian anthropogenic aerosol transported in the free troposphere over the Pacific Ocean found that the oxidation, inferred by the average oxygen to carbon ratio (O/C), continued to increase over the course of roughly a week 50 (Dunlea et al., 2009). In a study of biomass burning aerosol transported in the free troposphere across the North Atlantic Ocean, Dzepina et al. (2015) observed a relatively low O/C ratio (0.46 ± 0.13), considering the aerosol transport time of more than 10 days (Aiken et al., 2008). Dzepina et al. (2015) hypothesized that cloud processing and other oxidative processes led to the formation and subsequent removal of oxidized species, leaving behind the more persistent aerosol species. Other recent studies of long-range transported brown carbon (BrC) from biomass burning in the boundary layer found that the aging of aerosol led 55 to a near complete depletion of BrC within 24 hours (Forrister et al., 2015; Laing et al., 2016). The remaining BrC was found to lead to a 6 % increase of BrC over background levels and may represent the ubiquitous BrC present in the atmosphere far from the source (Forrister et al., 2015). This leftover BrC aerosol could impact large areas globally because much of it is located within the free troposphere and above clouds, due to the typically elevated injection heights of aerosol over wildfires (Val Martin et al., 2008a). These studies indicate that free tropospheric aerosol chemistry is particularly important because this 60 aerosol can have a longer atmospheric lifetime than boundary layer aerosol (Laing et al., 2016) allowing it to be transported over greater distances.

Studies of transported biomass burning aerosol are typically performed using instrumentation either onboard aircrafts (Capes et al., 2008) or located at low altitude (Bougiatioti et al., 2014; Vakkari et al., 2014) and continental mountain (Laing et al., 65 2016) sites. Aircraft measurements have the advantage of sampling aerosol over wide spatial and altitudinal ranges, but they are limited to short time periods, typically of a few days to a week (Capes et al., 2008; Dunlea et al., 2009). Ground sites are less constricted by time, but because of the high injection heights of wildfires, biomass burning aerosol are often above the boundary layer (Val Martin et al., 2008a). Thus, low altitude sites are less often affected by pyro-convective wildfire plumes-due to the high injection heights of wildfires (Val Martin et al., 2008a). Continental mountain sites typically have seasonally

70 limited access to the free troposphere, because high summer temperatures can lead to convection of the planetary boundary layer influence through convection (Collaud Coen et al., 2011). Thus, many of the continental mountain sites have long-term access to the free troposphere in the winter, but not in the summer when most wildfire activity occurs. The Pico Mountain Observatory (PMO, see the Supplement for additional information), is located 2225 m above sea level (a.s.l) on the caldera summit of Pico Mountain, on Pico Island in the Azores archipelago in the North Atlantic. The marine boundary layer in the region has been measured and is estimated to range from 500 to 2000 m a.s.l in the summer months (Kleissl et al., 2007; Remillard et al., 2012; Zhang et al., 2017), well below the observatory. This permits access to free tropospheric long-range transported aerosol during the wildfire season. This, in conjunction with negligible local emission sources, makes PMO an ideal site for the study of long-range transported free tropospheric aerosol.

80 As described by Zhang et al. (2017), the Azores-Bermuda anticyclone causes persistent downward mixing from the upper free troposphere and lower stratosphere, and is the dominant meteorological pattern in this region, and strengthens in the summer. The FLEXible PARTicle dispersion model (FLEXPART) retroplumes discussed in Zhang et al. (2017) show that this site is most commonly impacted by North American outflow (30-40%). In the summer months (June – August), 15% of the intercepted air masses have North American anthropogenic influence, and 7.3% have wildfire influence (Zhang et al., 2017).
85 These factors make PMO an excellent site for the study of North American outflow (Val Martin et al., 2008a). In many of the previous studies at PMO, investigators focused on the North American outflows of NO_x, NO_y, CH₄, non-methane hydrocarbons, and O₃ gases (Val Martin et al., 2006; Pfister et al., 2006; Val Martin et al., 2008a; Val Martin et al., 2008b; Helmig et al., 2015) and the physical characteristics of black carbon and mineral dust aerosol and their ice nucleation activity (Fialho et al., 2005; China et al., 2015; China et al., 2017). So far, only Dzepina et al. (2015) has previously looked at the 90 aerosol chemical and molecular characteristics of the organic aerosol collected at the site.

Recent environmental and laboratory studies have shown that under low temperature and low relative humidity (conditions common in the free troposphere), aerosol can be in a solid glassy phase (Zobrist et al., 2008; Virtanen et al., 2010). This 95 observation has been hypothesized to lead to longer atmospheric lifetimes for organic species that are otherwise susceptible to degradation through oxidative processes. As an example, polycyclic aromatic hydrocarbons (PAH) such as benzo[a]pyrene were observed to have a much higher ambient concentration than what could be explained by model simulations without considering the aerosol phase state (Shrivastava et al., 2017). Recently, PAH have been shown to enhance the formation of a viscous phase state in laboratory generated secondary organic aerosol (SOA) (Zelenyuk et al., 2017). Since PAH are common 100 products of biomass burning and anthropogenic emissions, the viscosity could be enhanced in ambient samples as well, leading to a greater likelihood of the occurrence of solid phase aerosol. The solid phase can increase the resistance of aerosol to photodegradation (Lignell et al., 2014; Hinks et al., 2015) and water diffusivity (Berkemeier et al., 2014), which may lead to lower rates of oxidation. Shiraiwa and colleagues developed a set of equations to predict the dry glass transition temperature based on the mass and O/C ratio of organic aerosol components (Shiraiwa et al., 2017; DeRieux et al., 2018). Thus, the phase 105 state of molecular species with respect to ambient conditions can be predicted using the Gordon-Taylor equation (Shiraiwa et al., 2017; DeRieux et al., 2018). Additionally, estimation methods to determine the volatility of organic aerosol were reported by Donahue et al. (2011) and Li et al. (2016). Both the phase state and volatility are potentially important in understanding the processes that affect aerosol during transport and aging. The low oxidation observed by Dzepina et al. (2015) was attributed to the dominance of persistent aerosol that resisted removal mechanisms, however it is possible that the phase state of the aerosol during transport played a significant role. The increased resistance to photodegradation (Lignell et al., 2014; Hinks et al., 2015) and water diffusivity (Berkemeier et al., 2014) of solid phase organic aerosol provide a basis for this hypothesis.

Ultrahigh resolution mass spectrometry (MS) is a necessary tool for determining the molecular characteristics of complex mixtures such as organic aerosol. It has been used to analyze dissolved organic matter (Kido-Soule et al., 2010; Herzsprung et al., 2014), cloud water (Zhao et al., 2013; Cook et al., 2017), fog water (Mazzoleni et al., 2010), sea spray (Schmitt-Kopplin et al., 2012), and organic aerosol (Walser et al., 2007; Mazzoleni et al., 2012; O'Brien et al., 2013; Wozniak et al., 2014; Dzepina et al., 2015). Ultrahigh resolution MS techniques are typically paired with electrospray ionization (ESI) because it is a soft ionization technique with little to no fragmentation of the molecular species being analyzed. Negative mode ESI is sensitive to molecules with acidic functional groups, which is ideal for the analysis of long-range transported organic aerosol due to its generally acidic nature (Bougiatioti et al., 2016). The ultrahigh mass resolution available from Fourier transform ion cyclotron resonance mass spectrometry (FT-ICR MS) and the high field Orbitrap Elite MS instruments ($R = 240,000$) separates sulfur containing species from carbon, hydrogen, and oxygen containing species (Schmitt-Kopplin et al., 2010), which is important because sulfur containing species are common in atmospheric aerosol (Schmitt-Kopplin et al., 2010; Mazzoleni et al., 2012; Dzepina et al., 2015).

The observations of Dzepina et al. (2015) raised interesting questions regarding the nature of long-range transported free tropospheric aerosol. To further elucidate the detailed molecular characteristics of free tropospheric aerosol, we analyzed three pollution events using ultrahigh resolution FT-ICR MS. We observed key molecular differences ~~in~~pertaining to the ~~extent of~~ oxidation likely related to the combination of transport pathways and their apparent emission sources. In this paper, we present the detailed molecular characteristics of organic aerosol collected at PMO and use the aerosol chemical composition, FLEXPART model simulations, and physical property estimates to interpret those characteristics and infer implications for long-range transported organic aerosol.

2 Methods

2.1 Sample collection

PM_{2.5} samples were collected at PMO on 8.5 x 10 in. quartz fiber filter using high volume air samplers (EcoTech HiVol 3000, Warren, RI, USA) operated at an average volumetric flow rate of 84 m³ hr⁻¹ for 24 h. Prior to sampling, the filters were wrapped in clean, heavy-duty aluminum foil and baked at 500 °C for ~ 8 hours to remove organic artifacts associated with the filters. Afterward, they were placed in antistatic sealable bags until deployment. We deployed four air samplers at the site, each was set up with a filter simultaneously and programmed to start one day after another, allowing for continuous sample collection for up to four consecutive days. This procedure was used to maximize the number of filters collected. Daily visits and maintenance were prohibited by the time consuming and strenuous hike necessary to reach the site. The sampled filters were removed and returned to the same aluminum wrapper and bag. The samples were then brought down the mountain and stored in a freezer until cold transport back to Michigan Tech where they were stored in a freezer until analysis. Three samples, collected in consecutive years at PMO, on 27-28 June 2013, 5-6 July 2014, and 20-21 June 2015 were analyzed in this study. The sampling time for all samples was 24 hours; on 27-28 June the sampling began at 19:00, on 5-6 July and on 20-21 June the sampling began at 15:00, all local times.

2.2 Chemical analyses

Organic carbon and elemental carbon (OC/EC) measurements were performed using an OC/EC analyzer (Model 4, Sunset Laboratory Inc. Tigard, OR, USA) following the NIOSH protocol. Major anions and cations were analyzed using ion chromatography. Anion analysis was performed using a Dionex ICS-2100 instrument (Thermo Scientific) with an AS-17-C analytical and guard column set (Thermo Scientific) using a KOH generator for gradient elution. Cation analysis was performed using a Dionex ICS-1100 instrument with CS-12A analytical and guard column set (Thermo Scientific) and an

isocratic 20 mM methanesulfonic acid eluent. The instruments were operated in parallel using split flow from the autosampler.

155 Additional details can be found in the Supplement.

2.3 Ultrahigh resolution FT-ICR mass spectrometry analysis

The samples for FT-ICR-MS analysis were selected based on the organic carbon concentration. Selected samples typically had more than 1000 µg of organic carbon per quartz filter. Sample preparation was described in detail in previous studies from our

160 group (Mazzoleni et al., 2010, 2012; Zhao et al., 2013; Dzepina et al., 2015). Briefly, one quarter of the quartz filter was cut into strips, placed in a pre-washed and baked 40 mL glass vial, and then extracted using ultrasonic agitation in Optima LC/MS grade deionized water (Fisher Scientific, Waltham, MA, USA) for 30 minutes. The extract was then filtered using a pre-baked

165 quartz filter syringe to remove undissolved material and quartz filter fragments. The sample filter was then sonicated again in 10 mL of Optima LC/MS grade deionized water for 30 minutes, filtered, and then added to the original 30 mL of filtrate

170 yielding a total of 40 mL. Ice packs were used during the sonication to ensure the water temperature stayed below 25 °C. The water-soluble organic carbon (WSOC) compounds were then isolated using Strata-X (Phenomenex, Torrance, CA, USA)

175 reversed phase solid phase extraction (SPE) cartridges to remove inorganic salts that can adduct with organic compounds during electrospray ionization. During the reversed phase SPE, losses of highly water soluble, low molecular weight (MW)

180 and hydrophobic, high MW organic compounds are expected. Thus, the resulting WSOC is the SPE-recovered fraction. The cartridges were pre-conditioned with acetonitrile and LC/MS grade water before the 40 mL filtrate was applied to the cartridges at a rate of ~ 1 mL/min. The cartridges were eluted with 2 mL of an aqueous acetonitrile solution (90/10 acetonitrile/water by volume) and stored in the freezer until analysis. The procedural loss of ionic low MW compounds such as oxalate can lead to an underprediction of the organic aerosol O/C and overprediction of the average glass transition temperatures (T_g). To investigate this, we used the concentrations of the prominent organic anions measured with ion chromatography to estimate

185 the abundance of these compound relative to the compounds detected by FT-ICR MS. The low MW [organic anion](#) corrected average O/C values correlated with the trends of the original O/C values, however the significance of impacts varies with the measured analyte concentrations and the assumptions associated with the uncertain mass fraction of the molecular formula

190 composition (Table SM4). When low MW organic anions were included in the estimated average dry T_g values, they dropped by ≤ 2.5 %, which was deemed relatively insignificant (Table SM5).

195 Ultrahigh resolution mass spectrometric analysis was done using FT-ICR MS with ESI at the Woods Hole Oceanographic Institution (Thermo Scientific LTQ Ultra). The samples were analyzed using direct infusion ESI in the negative ion mode.

200 Negative polarity is effective for the deprotonation of polar organic molecules (Mazzoleni et al., 2010), which are expected to dominate the organic aerosol mass fraction and were the focus of this study. The spray voltage ranged from 3.15 to 3.40 kV

205 depending on the ionization stability with a sample flow rate of 4 to 5 µL/min. We used a scan range of m/z 100 – 1000 with a mass resolving power of 400,000 (defined at m/z 400) for all samples. The samples were run in duplicate and 200 transient

210 scans were collected. The transients were co-added for each replicate run using the Midas Co-Add tool and molecular formula assignments were made using Composer software (Sierra Analytics), as described in previous studies (Mazzoleni et al., 2012;

215 Dzepina et al., 2015). The resulting molecular formula assignments underwent additional quality assurance (QA) data filtering to remove chemically unreasonable formulas with respect to O/C, hydrogen to carbon ratio (H/C), double bond equivalent

220 (DBE), and absolute PPM error as described in the Supplemental Information of Putman et al. (2012). Molecular formulas in common with the instrument blanks with signal intensity ratios < 3 were removed; meanwhile analytes in common with the

225 field blanks with signal intensity ratios < 3 were flagged. Specifically, two formulas ($C_{17}H_{34}O_4$ and $C_{19}H_{38}O_4$) observed in PMO-1 could not be classified as pertaining only to the field blank and so they were not removed. Further discussion about

195 the blank subtraction is provided in the Supplement. To produce the final data set for each sample, the replicates were aligned and only the molecular formulas found in both replicates after QA were retained.

2.4 FLEXPART numerical simulations

199 FLEXPART was used to determine the sources, ages, and transport pathways of the aerosol samples collected at PMO. 200 FLEXPART backward simulations (also called retroplumes) were driven by meteorology fields from the Global Forecast System (GFS) and its Final Analysis with 3-hour temporal resolution, 1° horizontal resolution, and 26 vertical levels. The 205 output was saved in a grid with a horizontal resolution of 1° latitude by 1° longitude, and eleven vertical levels from the surface to 15,000 m a.s.l. For each simulation, 80 thousand air parcels were released from the receptor and transported backwards for 210 20 days to calculate a source-receptor relationship (in units of $s\ kg^{-1}$, Seibert and Frank, 2004). FLEXPART retroplumes were 215 then multiplied with CO emission inventories ($kg\ s^{-1}$) from the Emissions Database for Global Atmospheric Research (EDGAR version 3.2 (Olivier and Berdowski, 2001)) and the Global Fire Assimilation System (Kaiser et al., 2012) to estimate the influence from anthropogenic and wildfire sources, respectively. The FLEXPART CO tracer calculated with this approach indicates the relative contributions from anthropogenic and biomass burning emissions. Since CO chemistry and dry deposition are not considered in the FLEXPART setup, the absolute FLEXPART CO value does not reproduce the actual CO 220 concentrations at Pico. FLEXPART does not consider the background CO accumulated in the atmosphere. The difference between FLEXPART CO and the actual CO largely depends on these factors. In previous applications of this approach, FLEXPART CO was able to estimate the episodes of CO enhancement due to transport of emissions (e.g., Brown et al., 2009; Stohl et al., 2007; Warneke et al., 2009). This approach has been used in several PMO studies and successfully captured elevated CO periods (e.g., Dzepina et al., 2015; Zhang et al., 2014; 2017) and it is used here to assist in the interpretation of 225 the chemical composition in this work.

226 In addition to the typical FLEXPART simulations done for the site (e.g., retroplume, CO source apportionment), we extracted 227 the ambient temperature and relative humidity (RH) from the GFS analysis data for model grids along the FLEXPART simulated 228 transport pathways. These parameters were then used to estimate the glass transition temperatures (T_g) of the organic 229 aerosol components during transport, based on its molecular composition from ultrahigh resolution MS, using estimation 230 methods recently developed by Shiraiwa et al. (2017) and extended to higher masses by DeRieux et al. (2018). DeRieux et al. 231 (2018) reported an uncertainty of ± 21 K for the prediction of any single compound, but the uncertainty is expected to decrease 232 when a mixture of compounds is considered. Nonetheless, we assumed an uncertainty range of ± 21 K on T_g and found that it 233 did not significantly change the T_g trends presented in Section 3.5. Further discussion on the uncertainty ~~on~~ of T_g is provided 234 in the Supplement. The distributions of the estimated organic aerosol component T_g values provides new insight for the 235 interpretation of long-range transported aerosol.

3 Results and discussion

3.1 Overview of the aerosol chemistry: OC/EC and IC

236 In this study, we present the detailed composition of three individual samples collected for 24 hours on 27-28 June 2013, 5-6 237 July 2014, and 20-21 June 2015 at the PMO. These samples, referred to as PMO-1, PMO-2 and PMO-3 hereafter, were selected 238 after analysis of organic and elemental carbon (OC/EC) were performed for all 127 aerosol samples collected in this study. 239 The three selected samples all had elevated organic carbon (OC) concentrations (Table 1) representing the capture of a 240 pollution plume. After blank subtraction, the median OC of the samples collected over the summers of 2013-2015 was $0.16 \pm$ 241 $0.018\ \mu g/m^3$. The minimum OC level measured was below the average blank concentration and the maximum was $2.07 \pm$ 242 $0.017\ \mu g/m^3$ (PMO-1). The most abundant anions and cations in these samples are also shown in Table 1. The presence of 243

these ions is consistent with the results of other studies (Yu et al., 2005; Aggarwal and Kawamura, 2009). Further discussion of the bulk chemical trends will be presented in a future manuscript.

240 The concentrations of common anions and cations can offer important insight regarding cloud processing and emission sources (Table 1). Specifically, the elevated level of sulfate observed in the PMO-2 sample can be an indicator of anthropogenic influence, cloud processing, or marine influence (Yu et al., 2005). We also observed elevated oxalate concentrations in PMO-1 and PMO-2. Oxalate is known to co-vary with sulfate concentrations in the atmosphere when they are formed by aerosol-245 cloud processing (Yu et al., 2005; Sorooshian et al., 2007). Thus, the oxalate to sulfate ratio can be an indication of cloud processing (Sorooshian et al., 2007); in general, a higher ratio is the result of increased cloud processing. As described in Sorooshian et al. (2007), the oxalate concentrations increase with cloud processing because there is more time for it to be produced, leading to an increased ratio. PMO-1 had the highest oxalate to sulfate ratio (0.278), followed by PMO-3 (0.124), and PMO-2 (0.084). The observed oxalate to sulfate ratios for these samples are all much higher than what was reported in Sorooshian et al. (2007) suggesting other factors may have impacted the ion concentrations. Specifically, an enrichment of 250 oxalate from biomass combustion plumes (Cao et al., 2017) likely contributed to the observed concentrations of these ions in PMO-1 and PMO-3. The bulk concentration of oxalate in PMO-2 is similar to PMO-1, but the sulfate in PMO-2 is much higher, leading to a low oxalate to sulfate ratio. Based on FLEXPART simulations it is likely that PMO-2 underwent aqueous phase processing (see Sect. 3.5), but the high concentration of sulfate from possible anthropogenic and marine sources appears to have obscured the oxalate-sulfate relationship (Yu et al., 2005; Sorooshian et al., 2007).

255 Despite inconsistencies in the replicate potassium measurements for PMO-1, elevated potassium levels were observed, indicating contributions from biomass combustion (Duan et al., 2004). PMO-3 had slightly elevated potassium relative to PMO-2, but not as high as PMO-1. Chloride was also present in PMO-1 and PMO-3, which has been shown in some studies to be a minor product of biomass burning, depending on the fuel burned (Levin et al., 2010; Liu et al., 2017).

260 The nitrate levels in PMO-2 were significantly lower than what was observed in PMO-1 and PMO-3, which is consistent with the observation that the marine boundary layer promotes the rapid removal of HNO_3 (Val Martin et al., 2008b). This is also consistent with removal due to cloud scavenging (Dunlea et al., 2009). The elevated nitrate in PMO-1 and PMO-3 is consistent with the observation of elevated NO_y and NO_x in the plumes of wildfire emissions made in previous studies at PMO (Val 265 Martin et al., 2008a) and a lack of recent cloud scavenging (Dunlea et al., 2009).

270 Despite the low altitude transport, the major ion concentrations in PMO-2 do not strongly support a major influence from marine sources (Quinn et al., 2015; Kirpes et al., 2017). However, the increased concentration of methane sulfonic acid (MSA) in PMO-2 relative to PMO-1 and PMO-3 suggests some degree of marine influence. To estimate this, we used the non- background subtracted sodium concentration as an upper limit to estimate sea salt sulfate according the method described in Chow et al. (2015), this led to a maximum sea salt sulfate contribution of 25 %. The influence of marine sources supports boundary layer transport. However, the results indicate that marine aerosol is not likely a major component of PMO-2, perhaps because the rate of PMO-2 transport was very fast.

275 **3.2 FLEXPART retroplume simulation results**

Representative FLEXPART retroplumes for the three samples are shown in Fig. 1, additional time periods are in the Supplement (Figs. S1-S3). PMO-1 was largely influenced by North American outflow transported relatively high in the free troposphere. Based on the FLEXPART carbon monoxide (CO) modeling (Fig. S4), PMO-1 was impacted by wildfire emissions

from Canada. The transport time for PMO-1 air masses from North America to PMO was about 7 days. The free tropospheric transport is likely due to the high injection heights (Val Martin et al., 2008a; 2010) of organic aerosol from wildfire events in northwestern Quebec (See Fig. S4, S5). Similar events at PMO have been identified previously by (Val Martin et al., 2006; 2008a). The air masses intercepted during PMO-3 were North American outflows that traveled in the lower free troposphere across the Northern Atlantic Ocean to Western Europe before circling back to PMO. The transport time for the PMO-3 air masses from North America to PMO was roughly 10 days. After a northward transport to Western Europe in the jet stream during the first 4-5 days, the simulated plume turned to the south and west, arriving at PMO from Europe in about 2-4 days. This air mass was most likely influenced by wildfire emissions in western and central Canada (U.S. Air Quality, Smog Blog. alg.umbc.edu). Similar to PMO-1, FLEXPART CO source apportionment (Fig. S4) suggests this sample was influenced by fire, although considering the OC concentration and transport time, it was much more diluted than what was observed in PMO-1. In contrast, the PMO-2 air masses traveled relatively low (≤ 2 km) over the “Rust Belt” (Illinois, Indiana, Michigan, Ohio, Pennsylvania, and New York) of the United States and stayed at approximately the same altitude until it reached the observatory 2-4 days later. This transport pattern suggests that the aerosol was predominantly transported in the boundary layer on its way to the PMO and was primarily influenced by a mixture of continental U.S. anthropogenic and biogenic emissions. This was supported by the FLEXPART CO simulations as well (Fig. S4). The height of the boundary layer over the continent generally ranges from 500-2500 m and is strongly affected by diurnal cycles, seasonal effects, and topography (Liu and Liang, 2010); overall, the continental boundary layer height generally increasing during the day and during the summer months. This suggests that PMO-2 was within the boundary layer over the United States.

3.3 Molecular formula oxidation metrics: O/C and OS_c

In this section, we describe the detailed molecular formula composition of the three individual samples PMO-1, PMO-2, and PMO-3. Overall, nearly 80% of the observed mass spectral peaks in the ultrahigh resolution mass spectra were assigned molecular formulas, which is comparable to previous studies (Zhao et al., 2013; Dzepina et al., 2015). After removing the duplicate molecular formulas containing ^{13}C or ^{34}S , a total of 3168 (PMO-1), 2121 (PMO-2), and 1820 (PMO-3) monoisotopic molecular formulas remained. Groups of molecular formulas were assigned based on their elemental composition $\text{C}_\text{c}\text{H}_\text{h}\text{N}_\text{n}\text{O}_\text{o}\text{S}_\text{s}$, including: carbon, hydrogen, and oxygen (CHO); carbon, hydrogen, nitrogen, and oxygen (CHNO); and carbon, hydrogen, oxygen, and sulfur (CHOS). The most frequently observed compositions were CHO and CHNO. The reconstructed negative ion mass spectra of the monoisotopic molecular formulas for each of the samples are provided in Fig. 2. Visual comparisons of the mass spectra indicate that PMO-2, which was likely transported through the North American continental and North Atlantic marine boundary layer, has aan increased prevalence of higher O/C ratio formulas compared to the two samples transported through the free troposphere. Considering the ion distribution and normalized relative abundances, PMO-1 and PMO-3 mass spectra look quite similar with a high frequency of individual O/C values < 0.5 . This may suggest similar emission sources or aerosol processing. In contrast, PMO-2 has a stronger relative influence of molecular compositions with higher O/C ratios. The O/C histogram plots in Fig. 2 provide additional evidence for the O/C differences between the two types of samples (free troposphere and boundary layer) due to the difference in the O/C distribution.

Although The North American boundary layer outflow of anthropogenic secondary organic aerosol captured in PMO-2 was likely influenced by SOA (Zhang et al., 2007) and thus is expected to have a higher initial O/C value compared to the pyro-convected wildfire emissions of biomass burning organic aerosol (e.g., Aiken et al., 2008; Jimenez et al., 2009; Bougiatioti et al., 2014). Although the initial compositions are unknown, we expected anticipated that the samples with longer transport times (~ 1 week for PMO-1 and PMO-3) would be at least similar or perhaps more oxidized than PMO-2 which had a much shorter transport time. However, this (~ 3 days). This expectation was based on results from aging studies of literature

describing secondary organic aerosol formation and aging (Volkamer et al., 2006; Jimenez et al., 2009) and the reported molecular composition of continental boundary layer anthropogenic aerosol (Mazzoleni et al., 2012; Huang et al., 2014). The lower oxidation observed in the free tropospheric samples transported for 7–10 days is consistent with our previous study at this site by reported in Dzepina et al. (2015). In fact, when we compared the molecular formula composition of the free tropospheric aerosol sample “9/24” from the study by Dzepina et al. (2015) to the free tropospheric samples in this study (PMO-1 and PMO-3), we observed that 86% and 91% of the molecular formulas are in common. FLEXPART simulations from both studies suggested indicated these samples were all affected by wildfire emissions, contributing to their similarity. In contrast, only 75% of the formulas found in the boundary layer sample (PMO-2) were common with those in Dzepina et al. (2015). These comparisons are provided in Table S2.

330

As observed in the mass spectra and histograms presented in Fig. 2, the samples have noticeable differences in the distribution of O/C values. This is also reflected in the abundance weighted mean O/C values for the samples: 0.48 ± 0.13 (PMO-1), 0.57 ± 0.17 (PMO-2), and 0.45 ± 0.11 (PMO-3). Note that these O/C values are averages of thousands of individual measurements, as such the standard deviation represents the range of values and not uncertainties (see Figs. S7-S8 for violin plots of the distributions). We also note that the relative abundance of compounds in ESI mass spectra is not directly proportional to their solution concentration, other factors including surface activity and polarity impact the ionization efficiency (Cech & Enke, 2001). Nonetheless, the abundance does differentiate trends between the samples and the assigned molecular formulas represent a collection of multifunctional isomers (e.g., LeClair et al., 2012). For completeness, both the abundance weighted average values for various metrics of aerosol oxidation and saturation (Table 2) and the unweighted average values (Table S3) are reported. Additional O/C distribution insight was derived from separating the species into CHO, CHNO, CHOS elemental groups. For example, the comparison of the species with CHO formulas in each sample indicates a smaller relative difference between PMO-2 aerosol compared to PMO-1 and PMO-3, with the PMO-2 aerosol having a higher average O/C value (0.55 ± 0.17 (PMO-2) compared to 0.47 ± 0.14 (PMO-1) and 0.44 ± 0.14 (PMO-3)). Meanwhile 85 - 98% of the CHO species in each sample are present in at least one other sample, with 848 (42 - 78%) of the formulas being found in all three samples, as shown in Fig. S9. This suggests that the CHO composition may be fairly uniform throughout the atmosphere, without a significant abundance of clear marker species after long-range transport, regardless of the source region and transport time. This observation is consistent with other studies which have observed the decay of marker species after ~ 24 hours (Bougiatioti et al., 2014; Forrister et al., 2015).

340

345

350

355

360

In contrast, the CHNO molecular formulas demonstrate stronger differences that correlate with the overall O/C ratio. The average O/C value for the CHNO formulas in PMO-2 was 0.59 ± 0.14 compared to 0.49 ± 0.15 in PMO-1 and 0.49 ± 0.14 PMO-3 (Table 2). Differences in the elemental ratios are often visualized using the van Krevelen plot, which shows the correlation of H/C vs. O/C. The van Krevelen plots for the three samples with the unique CHNO formulas present in each sample are shown in Fig. 3. Most of the unique CHNO species in PMO-2 (68%) fall in the more oxidized region of the plot (Tu et al., 2016) with high overall O/C values. This differs from the PMO-1 unique species that are predominantly on the less oxidized, low O/C side of the plot, or the oxidized aromatic region. Another observation from the CHNO species is more identified species in both PMO-1 (1120) and PMO-3 (608) than in PMO-2 (561), despite the higher total number of molecular species in PMO-2 compared to PMO-3. This is potentially due to the enrichment of NO_x and NO_y species as previously observed in wildfire pollution events (Val Martin et al., 2008a), which may in turn lead to an increased nitrogen content in the organic aerosol species. The nitrogen containing species show a distinct difference in terms of the total oxidation between the two sets of samples, more so than the CHO compounds. This implies that much of the distinction between different aerosol sources may come from heteroatom containing species.

The difference in O/C is even more evident in the sulfur containing formulas (CHOS). The PMO-2 CHOS species have a much higher average O/C ratio (0.74 ± 0.34) than what is observed in PMO-1 (0.48 ± 0.14). Consistent with the CHNO formulas, the PMO-2 unique CHOS formulas (55% of unique formulas) are present in the oxidized region of the plot, whereas those in PMO-1 are nearly completely in the less oxidized region of the van Krevelen plot (Fig. S10). The Kendrick plot (Fig. S10c) also demonstrates a clear difference between the two samples. Most of the unique CHOS compounds in PMO-2 are located on the lower mass, higher defect side of the plot, while the PMO-1 formulas are on the higher mass, lower defect side. This difference is due to the larger amount of oxygen present in the PMO-2 formulas, which would lead to a greater mass defect than the more reduced CHOS formulas present in PMO-1. Higher oxygen content of PMO-2 aerosol is supported by its higher O/C ratio when compared to PMO-1 as shown in box plots (Fig. S10d). Very few CHOS molecular formulas ($N = 29$) were identified in PMO-3 and most of them ($N = 26$ of 29 total) were also present in PMO-1. Due to the small number of identified CHOS formulas in [this samplePMO-3](#), we did not consider it in the comparison between CHOS formulas in the samples. [The overall](#) [The increased number of sulfur species observed in PMO-2 are likely associated with the anthropogenic emission sources in the North American boundary layer. Overall, the observed](#) differences [that are observed](#) in the O/C ratios between the boundary layer transported aerosol (PMO-2) compared to the free troposphere transported aerosol (PMO-1 and PMO-3) highlight [the](#) differences in the aging and lifetime of aerosol relative to its transport pathway- [and emission source.](#)

Another commonly used metric of aerosol oxidation is the average oxidation state of carbon (OS_C) described by Kroll et al. (2011). The average OS_C includes both hydrogen and oxygen for the average oxidation of carbon in each molecular formula. Additionally, we assumed all nitrogen and sulfur were present as nitrate and sulfate functional groups and calculated the OS_C with the appropriate corrections (Equation S1). The average OS_C values (Table 2) for the three samples show again that PMO-2 is more oxidized than the other two samples. The average OS_C values for the CHO formulas in PMO-1 and PMO-2 are very similar (Table 2), but as shown in the histograms in Fig. 4, their relative abundance distributions are quite different. The OS_C vs. carbon number plots in Fig. 4 show slight differences between PMO-1 and PMO-2, mostly in the distribution of the sulfur containing formulas. However, the similarity of the PMO-1 and PMO-3 samples and their difference from the PMO-2 sample is quite clear in the visual comparisons of the histograms of the OS_C values with their normalized relative abundances. The observation of an overall lower oxidation in PMO-1 and PMO-3 may support the findings of Aiken et al. (2008) and Bougiatioti et al. (2014) who reported that biomass burning aerosol are less oxidized than other types of aerosol, even after some aging. Conversely, the overall higher oxidation of PMO-2 implies that the sampled aerosol was likely more hygroscopic, included [better](#) [more efficient](#) cloud condensation nuclei (Massoli et al., 2010), [and](#) [or](#) had [components of a](#) less volatile [components](#) [nature](#) (Ng et al., 2011) than PMO-1 and PMO-3.

3.4 Molecular formula aromaticity and brown carbon

The aromaticity of the samples is also different between the two groups of aerosol [samples](#). Based on the aromaticity index (AI, Eq. S2; AI_{mod}, Eq. S3; Koch and Dittmar, 2006; 2016), the free tropospheric aerosol samples (PMO-1 and PMO-3) are more aromatic than the convected boundary layer aerosol (PMO-2; Fig. 5). The presence of more aromatic species in the long-range transported wildfire-influenced aerosol may lead to increased light absorption (Bao et al., 2017) [or](#) [and](#) [perhaps an](#) [increased](#) resistance to oxidation (Perraudin et al., 2006). Aromatic species can also be associated with the presence of brown carbon (BrC; Desyaterik et al., 2013). Aromaticity is heavily dependent on the H/C ratio and the DBE (Eq. S4), where low H/C and high DBE indicate aromatic structure. Histograms depicting the distribution of H/C and DBE values for the three samples are shown in Fig. S11. As observed previously, PMO-1 and PMO-3 are more similar to each other than compared to PMO-2. Likewise, PMO-1 and PMO-3 exhibit an increase in the number frequency of higher DBE species, which is not

405 observed in PMO-2, supporting the observation of an increased overall aromaticity for these free tropospheric aerosol [samples](#). Many aromatic compounds, such as PAH are known to be carcinogens, and are a product of incomplete combustion biomass burning and anthropogenic emissions (Perraudin et al., 2006; Bignal et al., 2008).

410 Generally, BrC is considered to be aromatic or olefinic in nature (Bao et al., 2017). In our observations, the two samples influenced by wildfire show the greatest amount of olefinic and aromatic species, which is likely associated with the presence of BrC compounds. Additional evidence for the presence of BrC in PMO-1 comes from aethalometer measurements using the 7 wavelength aethalometer (Magee Scientific Company, Berkeley, California, USA) located at the site, which detected a wavelength-dependent peak with an Ångström [coefficient exponent](#) of 1.3 during the sampling period. Ångström [coefficients](#) above 1 suggest the presence of BrC or iron oxides. Based on the retroplume analysis and comparison to similar samples (Dzepina et al., 2015), the detected peak is most likely the result of BrC. Figure S12 contains the aethalometer observations for this event. Difficulties with the instrument prevented similar data from being collected for PMO-3, although based on the retroplumes, ambient conditions, and molecular characteristics similar results seem likely. In addition to the aethalometer response, PMO-1 contained species that were related to BrC in studies by Iinuma et al. (2010) and Lin et al. (2016) (Table S4). This observation provides evidence for the persistence of BrC species, which is contrary to the 415 observations by Forrister et al. (2015) who concluded that BrC is mostly removed within 24 hours. Additionally, the high concentration of OC for this sample makes it seem unlikely that we observed just a minor residual fraction. Perhaps, the lifetime of BrC is dependent on additional ambient conditions that influence aerosol oxidation and phase state.

3.5 Phase state, volatility, and cloud processing: Implications for the observed aerosol oxidation

425 Atmospheric aging processes are influenced by ambient conditions, such as temperature and water vapor, and the concentrations of reactive species. Recently, Shrivastava et al. (2017) reported observations of long-range transported PAH from Asia to North America and suggested an enhanced lifetime due to a probable glassy aerosol phase state during transport. Additionally, model simulations reported by Shiraiwa et al. (2017) indicated that model SOA is predicted to be semi-solid or 430 glassy at altitudes above 2000 m in the northern hemisphere. Since the PMO aerosol was sampled at 2225 m above sea level, we examined the estimated glass transition temperature (T_g) of the studied WSOC species in addition to the markers of aqueous phase processing for the three PMO samples. Increased aerosol viscosity has been shown to decrease the rate of photodegradation (Lignell et al., 2014; Hinks et al., 2015) and water diffusivity (Berkemeier et al., 2014). Both photodegradation and water diffusion are expected to strongly affect the oxidation and aging of aerosol species during 435 transport.

435 In general, lower volatility typically inversely correlates with T_g (Shiraiwa et al., 2017) and viscosity. As such it was important to estimate the volatility of the PMO aerosol. Using the parameters reported by Donahue et al. (2011) and Li et al. (2016), we estimated the volatility of the FT-ICR MS identified organic aerosol molecular compositions (Figs. S13 and S14, respectively). As expected based on the length of transport for the samples, the majority of formulas show extremely low volatility. 440 Interestingly, PMO-2 has a larger number of higher abundance molecular formulas with extremely low volatility and elevated oxidation relative to PMO-1 and PMO-3 (Fig. 6). This highlights the relationship between O/C and volatility, where volatility is expected to decrease as O/C increases when the mass range is constant (Ng et al., 2011); the relationship between oxygen and carbon and its effect on volatility is used by both Donahue et al. (2011) and Li et al. (2016) to estimate volatility. Similarly, lower volatility is expected to lead to lower diffusivity in aerosol even at elevated RH as demonstrated by Ye et al. (2016).

As predicted in earlier studies (Shrivastava et al., 2017 and Shiraiwa et al., 2017), particles transported in the free troposphere are likely semi-solid to solid, where the actual particle viscosity depends on the ambient conditions and the composition of the particles. Thus, to better understand the potential phase state associated with the PMO organic aerosol, we first estimated the dry T_g for the identified CHO molecular formulas in each of the PMO aerosol using the estimation method by DeRieux et al. (2018; Eq. S5). We then converted the dry T_g to the RH dependent T_g (below). Currently T_g can only be estimated for CHO species, however the CHO species were the most frequently observed and constituted a major fraction of the total relative abundance in the PMO negative ion mass spectra. Assuming the identified CHO compositions are fairly representative of the total organic aerosol composition, a comparison of the T_g values to the ambient temperature (T_{amb}) provides an indication of the likely phase state of the organic aerosol particles. Generally, if T_g exceeds T_{amb} , a glassy solid state is predicted, likewise, if T_g is less than T_{amb} then either a semi-solid or liquid state is predicted depending on the ratio magnitude (Shiraiwa et al., 2017; DeRieux et al., 2018). Although the exact composition of the total organic aerosol is yet unknown, the identified water-soluble organic compounds provide a reasonable upper limit for the estimated T_g values. Under this assumption, the CHO molecular formulas in PMO-1 and PMO-3 had higher average dry T_g values than PMO-2 (Table S5, Fig. S16), which implies that they would be more viscous than PMO-2, given similar atmospheric conditions.

Water is known to be a strong plasticizer relative to typical aerosol species (Koop et al., 2011; Shiraiwa et al., 2017; Reid et al., 2018), thus it can decrease T_g and the overall aerosol viscosity. Therefore, it's important to consider the ambient relative humidity when estimating the T_g . Using the extracted ambient temperature and RH from the GFS along the FLEXPART retroplumes and the Gordon-Taylor equation (Eqs. S6 - S7), the calculated dry T_g were modified to RH-dependent T_g for the CHO molecular species. The distributions of the T_g values for the three PMO samples based on one standard deviation of the ambient conditions are shown as boxplots in Fig. 7. The range of ambient temperature and RH extracted from the GFS along the FLEXPART simulated path yields a wide range of T_g values (Figs. 7, S17). The estimates were taken back only 5 days due to the increasing range of possible meteorological conditions associated with the spread in the air masses as shown in Figs. 1 and S1-S3. Overall, the distributions of T_g values in PMO-1 and PMO-3 generally exceed the ambient temperature (Fig. 7), implying that particles containing a majority of these compounds would likely be solid. To account for the low molecular weight organic anions not observed in the FT-ICR mass spectra, their mass concentrations and T_g values (estimated using the Boyer-Kauzmann rule (Koop et al., 2011; Shiraiwa et al., 2017; DeRieux et al., 2018)) are also shown in Fig. 7. The three most prevalent low molecular weight organic acids indicate the potential impact of those compounds on the overall T_g value of a particle that contains them. Oxalic acid was estimated to have a similar T_g value to a majority of the higher MW species identified in PMO-2, but it is slightly lower than the majority of species in PMO-1 and PMO-3. However, the mass fraction of oxalate is 3 times lower in PMO-1 and PMO-3 (2.3 and 3.0 %) compared to PMO-2 (9.4 %).

The results suggest that aerosol in PMO-1 and PMO-3 was overall less susceptible to atmospheric oxidation due to the aerosol phase state during free tropospheric long-range transport than it may have been in the boundary layer with higher ambient RH and temperature. A more viscous phase state during transport may also explain the presence of persistent BrC species in PMO-1, where the BrC species are protected from oxidation similarly to the long-lived PAHs observed by Shrivastava et al. (2017). In contrast to the observations from PMO-1 and PMO-3, much of the PMO-2 T_g distribution falls below the ambient temperature indicating implying a semi-solid or liquid state during the final 5 days of transport. This indicates an increased susceptibility to oxidation processes in the atmosphere (Shiraiwa et al., 2011), such as aqueous phase processing. The possibility of aqueous phase processing is also supported by the extracted GFS RH in Fig. 7, which is above 50% for the last 5 days of PMO-2 transport. The potential for liquid/semi-solid aerosol in the boundary layer is consistent with other studies (Shiraiwa et al., 2017; Maclean et al., 2017) and is expected based on due to the increased RH in the boundary layer and the

plasticizing effect of water. Although, we note the PMO-2 average dry T_g values were 4-5° lower than those of PMO-1 and PMO-3. The overall, the estimates of dry T_g and RH-dependent T_g provide an otherwise unattainable upper limit estimate of the aerosol phase state of the sampled free tropospheric aerosol in this study.

As described above, the most obvious difference in the molecular composition of PMO-2 vs. PMO-1 and PMO-3 is the increased extent of oxidation. In fact, most of the unique species observed in PMO-2 are in the highly oxidized region of the van Krevelen plot (Fig. 8). However, the exact oxidation pathways that led to the increased oxidation observed for PMO-2 and its initial composition are unclear. Both gas phase and aqueous phase reactions lead to SOA, where aqueous SOA components can have higher O/C values than gas phase SOA components (Lim et al., 2010; Ervens et al., 2011). The high numbers of CHNO and CHOS molecular formulas observed here are consistent with secondary components associated with an emission plume likely enriched in SO_2 , NO_x , and O_3 pertaining to its expected anthropogenic influence. All three of these reactive species have been shown to lead to production and oxidation of SOA in the atmosphere (Hoyle et al., 2016; Bertrand et al., 2018). Cloud and aqueous processing have also been shown to increase the oxidation of atmospheric organic matter (e.g., Ervens et al., 2008; Zhao et al., 2013; Cook et al., 2017). Therefore, aqueous phase oxidation may have contributed to the higher oxidation observed in PMO-2 despite its more rapid transport from North America to the PMO; Brege et al., 2018. In fact, most of the unique species observed in PMO-2 are in the highly oxidized region of the van Krevelen plot (Fig. 8). Comparisons of the detailed molecular composition of the PMO samples with studies of cloud (Zhao et al., 2013; Cook et al., 2017) and fog (Mazzoleni et al., 2010) water organic matter indicate that the formulas uniquely common to only PMO-2 and the literature atmospheric water samples have higher O/C consistent with, which supports aqueous phase processing during transport. These results are provided in Fig. S19 and Table S6. Studies have shown that the reactive species emitted from anthropogenic plumes (SO_2 , NO_x , O_3) can play a role in the oxidation of the organic species that are dissolved in water (Blando and Turpin, 2000; Chen et al., 2008; Ervens et al., 2011); furthermore, studies have shown aerosol liquid water content contributes to aqueous production of SOA (Volkamer et al., 2009; Lim et al., 2010). The elevated RH extracted from the GFS for this plume (Fig. 7) indicates the presence of aerosol liquid water and is consistent with its ubiquitous nature (Nguyen et al., 2016). Additionally, PMO-2 had a strongly elevated non-sea salt sulfate concentration relative to PMO-1 and PMO-3, which supports cloud also indicates aqueous phase processing. Oxalate, a marker of cloud processing (Crahan et al., 2004; Yu et al., 2005; Sorooshian et al., 2007; Hoyle et al., 2016). Oxalate, another well-known marker of potential aqueous phase processing (Warneck 2003; Crahan et al., 2004; Yu et al., 2005; Sorooshian et al., 2007; Carlton et al., 2007), was also elevated in PMO-2. The organic mass fraction of oxalate was 9.4 % in PMO-2 compared to 2.3 % and 3.0 % in PMO-1 and PMO-3. Furthermore, nitrate is known to be scavenged during cloud processing (Dunlea et al., 2009), leading to its decrease in recently cloud processed aerosol. The nitrate concentration in PMO-2 was very low compared to PMO-1 or PMO-3 (Table 1), supporting the idea of cloud scavenging in PMO-2. Overall, the molecular aqueous phase processed aerosol in PMO-2. While clearly gas phase SOA cannot be excluded, several lines of evidence suggest that aqueous phase oxidation likely influenced the chemical and physical characteristics and of the PMO-2 aerosol to a larger extent than those of PMO-1 and PMO-3 based on the observed molecular characteristics, major ion concentrations (Fig. S20) indicate that PMO-2 was likely affected by aqueous phase oxidation during transport, and the model simulated transport pathways and GFS meteorology.

4 Conclusions

Aerosol samples collected on 27-28 June 2013 (PMO-1), 5-6 July 2014 (PMO-2), and 20-21 June 2015 (PMO-3) at the Pico Mountain Observatory were analyzed using ultrahigh resolution FT-ICR mass spectrometry for molecular formula composition determination. FLEXPART retroplumes for the sampled air masses indicate that: (a) PMO-1 and PMO-3 aerosol

575 were transported predominantly through the free troposphere and were primarily influenced by wildfire emissions; and (b) PMO-2 aerosol were transported primarily through the boundary layer over the Northeast continental U.S. and the North Atlantic Ocean ~~before being intercepted at the observatory and was largely influenced by anthropogenic and biogenic sources.~~ Although elevated levels of OC, sulfate, and oxalate were found in all three samples, PMO-2 had the overall highest mass fractions of oxalate and sulfate, indicating a clear influence of aqueous phase processing. The molecular formula assignments 580 indicated differences in the aerosol oxidation between the free troposphere transported aerosol (PMO-1 and PMO-3) and the boundary layer transported aerosol (PMO-2). These observations suggest that the transport pathways, in addition to the emission sources, ~~contribute contributed~~ to the observed differences in the organic aerosol oxidation. The ambient temperature and RH at upwind times were extracted from the GFS analysis in FLEXPART and were used to estimate the glass transition temperatures of the aerosol species during transport. The results suggest that the organic aerosol components extracted from 585 PMO-1 and PMO-3 were considerably more viscous due to lower RH than those from PMO-2 and thus were less susceptible to aqueous phase oxidation. The concept of increased relationship between aerosol viscosity leading and its susceptibility to less oxidation ~~of aerosol~~ in the free troposphere is well supported ~~in the literature~~ (e.g., Koop et al., 2011; Berkemeier et al., 2014; Lignell et al., 2014; Shiraiwa et al., 2017). This suggests that biomass burning emissions and BrC injected into the free 590 troposphere are more resistant to removal than aerosol transported in the boundary layer, due largely to the ambient conditions in the free troposphere. ~~More~~Although more work is needed to better constrain the molecular composition of long-range transported aerosol and the processes that affect it during transport. ~~The, the~~ The presented results have broader implications for the aging of long-range transported ~~biomass burning organic~~ aerosol rapidly convected to the free troposphere.

Data availability

595 The molecular formula composition for each sample in this study is available via Digital Commons at the following link: <http://digitalcommons.mtu.edu/chemistry-fp/88/>.

Acknowledgements

This project was supported with funding from NSF (AGS-1110059) and DOE (DE-SC0006941). Logistical support for the 600 operation of the Pico Mountain Observatory was provided by the Regional Secretariat of the Environment and the Sea of the Portuguese Regional Government of the Azores. Major equipment cost share and graduate student support associated with this project was provided by the Earth, Planetary, and Space Science Institute at Michigan Technological University. We thank Mike Dziobak, Kendra Wright, Sumit Kumar, Andrea Baccarini, Stefano Viviani, Jacques Huber, and Detlev Helmig for assistance in the field. We thank Manabu Shiraiwa, Sarah Petters, and Marcus Petters for helpful discussion regarding aerosol 605 phase state. Finally, we thank Melissa Soule and Elizabeth Kujawinski of the Woods Hole Oceanographic Institution (WHOI) Mass Spectrometry Facility for FT-ICR MS instrument time and assistance with data acquisition (NSF OCE-0619608 and Gordon and Betty Moore Foundation).

References

610 Aggarwal, S. G. and Kawamura, K.: Carbonaceous and inorganic composition in long-range transported aerosols over northern Japan: Implication for aging of water-soluble organic fraction, *Atmos. Env.*, 43(16), 2532–2540, doi:10.1016/j.atmosenv.2009.02.032, 2009.

Aiken, A. C., DeCarlo, P. F., Kroll, J. H., Worsnop, D. R., Huffman, J. A., Docherty, K. S., Ulbrich, I. M., Mohr, C., Kimmel, J. R., Sueper, D., Sun, Y., Zhang, Q., Trimborn, A., Northway, M., Ziemann, P. J., Canagaratna, M. R., 615 Onasch, T. B., Alfarra, M. R., Prevot, A. S. H., Dommen, J., Duplissy, Metzger, A., Baltensperger, U., and Jimenez J. L.: O/C and OM/OC Ratios of Primary, Secondary, and Ambient Organic Aerosols with High-Resolution Time-of-Flight Aerosol Mass Spectrometry, *Environ. Sci. Technol.*, 42(12), 4478–4485, doi:10.1021/es703009q, 2008.

Arangio, A. M., Slade, J. H., Berkemeier, T., Pöschl, U., Knopf, D. A. and Shiraiwa, M.: Multiphase Chemical Kinetics of OH Radical Uptake by Molecular Organic Markers of Biomass Burning Aerosols: Humidity and Temperature

[Dependence, Surface Reaction, and Bulk Diffusion, J. Phys. Chem., 119\(19\), 4533–4544, doi:10.1021/jp510489z, 2015.](#)

Bao, H., Niggemann, J., Luo, L., Dittmar, T. and Kao, S.: Aerosols as a source of dissolved black carbon to the ocean, *Nat. Commun.*, 8(1), 510, doi:10.1038/s41467-017-00437-3, 2017.

Berkemeier, T., Shiraiwa, M., Pöschl, U. and Koop, T.: Competition between water uptake and ice nucleation by glassy organic aerosol particles, *Atmos. Chem. Phys.*, 14(22), 12513–12531, doi:10.5194/acp-14-12513-2014, 2014.

Berkemeier, T., Steimer, S., Krieger, U., Peter, T., Pöschl, U., Ammann, M. and Shiraiwa, M.: Ozone uptake on glassy, semi-solid and liquid organic matter and the role of reactive oxygen intermediates in atmospheric aerosol chemistry, *Phys. Chem. Chem. Phys.*, 18(18), 12662–12674, doi:10.1039/c6cp00634e, 2016.

[Bertrand, A., Stefenelli, G., Jen, C. N., Pieber, S. M., Bruns, E. A., Ni, H., Temime-Roussel, B., Slowik, J. G., Goldstein, A. H., Haddad, I. E., Baltensperger, U., Prévôt, A. S. H., Wortham, H. and Marchand, N.: Evolution of the chemical fingerprint of biomass burning organic aerosol during aging, Atmos. Chem. Phys., 18\(10\), 7607–7624, doi:10.5194/acp-18-7607-2018, 2018.](#)

Bignal, K. L., Langridge, S. and Zhou, J. L.: Release of polycyclic aromatic hydrocarbons, carbon monoxide and particulate matter from biomass combustion in a wood-fired boiler under varying boiler conditions, *Atmos. Env.*, 42(39), 8863–8871, doi:10.1016/j.atmosenv.2008.09.013, 2008.

[Blando, J. D. and Turpin, B. J.: Secondary organic aerosol formation in cloud and fog droplets: a literature evaluation of plausibility, Atmos. Environ., 34\(10\), 1623–1632, doi:10.1016/s1352-2310\(99\)00392-1, 2000.](#)

Bougiatioti, A., Stavroulas, I., Kostenidou, E., Zarmpas, P., Theodosi, C., Kouvarakis, G., Canonaco, F., Prevot, A. S. H., Nenes, A., Pandis, S. N. and Mihalopoulos, N.: Processing of biomass-burning aerosol in the eastern Mediterranean during summertime, *Atmos. Chem. Phys.*, 14(9), 4793–4807, doi:10.5194/acp-14-4793-2014, 2014.

Bougiatioti, A., Nikolaou, P., Stavroulas, I., Kouvarakis, G., Weber, R., Nenes, A., Kanakidou, M. and Mihalopoulos, N.: Particle water and pH in the eastern Mediterranean: source variability and implications for nutrient availability, *Atmos. Chem. Phys.*, 16(7), 4579–4591, doi:10.5194/acp-16-4579-2016, 2016.

[Brege, M., Paglione, M., Gilardoni, S., Decesari, S., Facchini, M. C., and Mazzoleni, L. R.: Molecular insights on aging and aqueous phase processing from ambient biomass burning emissions-influenced Po Valley fog and aerosol, Atmos. Chem. Phys., in press, 2018.](#)

Brown, S. S., deGouw, J. A., Warneke, C., Ryerson, T. B., Dubé, W. P., Atlas, E., Weber, R. J., Peltier, R. E., Neuman, J. A., Roberts, J. M., Swanson, A., Flocke, F., McKeen, S. A., Brioude, J., Sommariva, R., Trainer, M., Fehsenfeld, F. C. and Ravishankara, A. R.: Nocturnal isoprene oxidation over the Northeast United States in summer and its impact on reactive nitrogen partitioning and secondary organic aerosol, *Atmos. Chem. Phys.*, 9(9), 3027–3042, doi:10.5194/acp-9-3027-2009, 2009.

Cao, F., Zhang, S., Kawamura, K., Liu, X., Yang, C., Xu, Z., Fan, M., Zhang, W., Bao, M., Chang, Y., Song, W., Liu, S., Lee, X., Li, J., Zhang, G., and Zhang, Y.: Chemical characteristics of dicarboxylic acids and related organic compounds in PM2.5 during biomass-burning and non-biomass-burning seasons at a rural site of Northeast China, *Environ. Pollut.*, 231(Pt 1), 654–662, doi:10.1016/j.envpol.2017.08.045, 2017.

Capes, G., Johnson, B., McFiggans, G., Williams, P. I., Haywood, J. and Coe, H.: Aging of biomass burning aerosols over West Africa: Aircraft measurements of chemical composition, microphysical properties, and emission ratios, *J. Geophys. Res-Atmos.*, 113(D23), doi:10.1029/2008jd009845, 2008.

[Carlton, A. G., Turpin, B. J., Altieri, K. E., Seitzinger, S., Reff, A., Lim, H.-J. and Ervens, B.: Atmospheric oxalic acid and SOA production from glyoxal: Results of aqueous photooxidation experiments, Atmos. Environ., 41\(35\), 7588–7602, doi:10.1016/j.atmosenv.2007.05.035, 2007.](#)

Cech, N. B. and Enke, C. G.: Practical implications of some recent studies in electrospray ionization fundamentals, *Mass Spec. Rev.*, 20(6), 362–387, doi:10.1002/mas.10008, 2001.

[Chen, Z. M., Wang, H. L., Zhu, L. H., Wang, C. X., Jie, C. Y. and Hua, W.: Aqueous-phase ozonolysis of methacrolein and methyl vinyl ketone: a potentially important source of atmospheric aqueous oxidants, Atmos. Chem. Phys., 8\(8\), 2255–2265, doi:10.5194/acp-8-2255-2008, 2008.](#)

China, S., Scarnato, B., Owen, R. C., Zhang, B., Ampadu, M. T., Kumar, S., Dzepina, K., Dziobak, M. P., Fialho, P., Perlinger, J. A., Hueber, J., Helmig, D., Mazzoleni, L.R. and Mazzoleni, C.: Morphology and mixing state of aged soot particles at a remote marine free troposphere site: Implications for optical properties, *Geophys. Res. Lett.*, 42(4), 1243–1250, doi:10.1002/2014gl062404, 2015.

China, S., Alpert, P. A., Zhang, B., Schum, S., Dzepina, K., Wright, K., Owen, R. C., Fialho, P., Mazzoleni, L.R., Mazzoleni, C., and Knopf, D. A.: Ice cloud formation potential by free tropospheric particles from long-range transport over the Northern Atlantic Ocean, *J. Geophys. Res-Atmos.*, 122(5), 3065–3079, doi:10.1002/2016jd025817, 2017.

730 Chow, J. C., Lowenthal, D. H., Chen, L.W.A., Wang, X., and Watson, J. G.: Mass reconstruction methods for PM2.5: a review, *Air Qual. Atmos. Hlth.*, 8(3), 243–263, doi:10.1007/s11869-015-0338-3, 2015.

735 Collaud Coen, M., Weingartner, E., Furger, M., Nyeki, S., Prevot, A. S. H., Steinbacher, M. and Baltensperger, U.: Aerosol climatology and planetary boundary influence at the Jungfraujoch analyzed by synoptic weather types, *Atmos. Chem. Phys.*, 11(12), 5931–5944, doi:10.5194/acp-11-5931-2011, 2011.

740 Cook, R. D., Lin, Y.-H., Peng, Z., Boone, E., Chu, R. K., Dukett, J. E., Gunsch, M. J., Zhang, W., Tolic, N., Laskin, A. and Pratt, K. A.: Biogenic, urban, and wildfire influences on the molecular composition of dissolved organic compounds in cloud water, *Atmos. Chem. Phys.*, 17(24), 15167–15180, doi:10.5194/acp-17-15167-2017, 2017.

745 Corrigan, A. L., Russell, L. M., Takahama, S., Äijälä, M., Ehn, M., Junninen, H., Rinne, J., Petäjä, T., Kulmala, M., Vogel, A. L., Hoffmann, T., Ebbin, C. J., Geiger, F. M., Chhabra, P., Seinfeld, J. H., Worsnop, D. R., Song, W., Auld, J. and Williams, J.: Biogenic and biomass burning organic aerosol in a boreal forest at Hyytiälä, Finland, during HUMPPA-COPEC 2010, *Atmos. Chem. Phys.*, 13(24), 12233–12256, doi:10.5194/acp-13-12233-2013, 2013.

750 Crahan, K. K., Hegg, D., Covert, D. S. and Jonsson, H.: An exploration of aqueous oxalic acid production in the coastal marine atmosphere, *Atmos. Environ.*, 38(23), 3757–3764, doi:10.1016/j.atmosenv.2004.04.009, 2004.

755 DeRieux, W.-S. W., Li, Y., Lin, P., Laskin, J., Laskin, A., Bertram, A. K., Nizkorodov, S. A. and Shiraiwa, M.: Predicting the glass transition temperature and viscosity of secondary organic material using molecular composition, *Atmos. Chem. Phys.*, 18(9), 6331–6351, doi:10.5194/acp-18-6331-2018, 2018.

760 Desyaterik, Y., Sun, Y., Shen, X., Lee, T., Wang, X., Wang, T. and Collett, J. L.: Speciation of “brown” carbon in cloud water impacted by agricultural biomass burning in eastern China, *J. Geophys. Res.-Atmos.*, 118(13), 7389–7399, doi:10.1002/jgrd.50561, 2013.

765 Donahue, N., Epstein, S., Pandis, S. and Robinson, A.: A two-dimensional volatility basis set: 1. organic-aerosol mixing thermodynamics, *Atmos. Chem. Phys.*, 11(7), 3303–3318, doi:10.5194/acp-11-3303-2011, 2011.

770 Duan, F., Liu, X., Yu, T. and Cachier, H.: Identification and estimate of biomass burning contribution to the urban aerosol organic carbon concentrations in Beijing, *Atmos. Env.*, 38(9), 1275–1282, doi:10.1016/j.atmosenv.2003.11.037, 2004.

775 Dunlea, E. J., DeCarlo, P. F., Aiken, A. C., Kimmel, J. R., Peltier, R. E., Weber, R. J., Tomlinson, J., Collins, D. R., Shinozuka, Y., McNaughton, C. S., Howell, S. G., Clarke, A. D., Emmons, L. K., Apel, E. C., Pfister, G. G., van Donkelaar, A., Martin, R. V., Millet, D. B., Heald, C. L. and Jimenez, J. L.: Evolution of Asian aerosols during transpacific transport in INTEX-B, *Atmos. Chem. Phys.*, 9(19), 7257–7287, doi:10.5194/acp-9-7257-2009, 2009.

780 Dzepina, K., Mazzoleni, C., Fialho, P., China, S., Zhang, B., Owen, R. C., Helmig, D., Hueber, J., Kumar, S., Perlinger, J. A., Kramer, L. J., Dziobak, M. P., Ampadu, M. T., Olsen, S., Wuebbles, D. J., and Mazzoleni, L. R.: Molecular characterization of free tropospheric aerosol collected at the Pico Mountain Observatory: a case study with a long-range transported biomass burning plume, *Atmos. Chem. Phys.*, 15(9), 5047–5068, doi:10.5194/acp-15-5047-2015, 2015.

785 Ervens, B., Cubison, M., Andrews, E., Feingold, G., Ogren, J. A., Jimenez, J. L., DeCarlo, P. and Nenes, A.: Prediction of cloud condensation nucleus number concentration using measurements of aerosol size distributions and composition and light scattering enhancement due to humidity, *J. Geophys. Res. Atmos.*, 112(D10), doi:10.1029/2006jd007426, 2007.

790 Ervens, B., Carlton, A. G., Turpin, B. J., Altieri, K. E., Kreidenweis, S. M., and Feingold, G.: Secondary organic aerosol yields from cloud-processing of isoprene oxidation products, *Geophys. Res. Lett.*, 35(2), doi:10.1029/2007gl031828, 2008.

795 Ervens, B., Turpin, B. J. and Weber, R. J.: Secondary organic aerosol formation in cloud droplets and aqueous particles (aqSOA): a review of laboratory, field and model studies, *Atmos. Chem. Phys.*, 11(21), 11069–11102, doi:10.5194/acp-11-11069-2011, 2011.

800 Fialho, P., Hansen, A. D. A. and Honrath, R. E.: Absorption coefficients by aerosols in remote areas: a new approach to decouple dust and black carbon absorption coefficients using seven-wavelength Aethalometer data, *J. Aerosol Sci.*, 36(2), 267–282, doi:10.1016/j.jaerosci.2004.09.004, 2005.

805 Forrister, H., Liu, J., Scheuer, E., Dibb, J., Ziembka, L., Thornhill, K. L., Anderson, B., Diskin, G., Perring, A. E., Schwarz, J. P., Campuzano-Jost, P., Day, D. A., Palm, B. B., Jimenez, J. L., Nenes, A. and Weber, R. J.: Evolution of brown carbon in wildfire plumes, *Geophys. Res. Lett.*, 42(11), 4623–4630, doi:10.1002/2015gl063897, 2015.

810 George, I. J. and Abbatt, J. P. D.: Heterogeneous oxidation of atmospheric aerosol particles by gas-phase radicals, *Nat. Chem.*, 2(9), nchem.806, doi:10.1038/nchem.806, 2010.

815 Helmig, D., Muoz, M., Hueber, J., Mazzoleni, C., Mazzoleni, L., Owen, R. C., Val-Martin, M., Fialho, P., Plass-Duelmer, C., Palmer, P. I., Lewis, A. C. and Pfister, G.: Climatology and atmospheric chemistry of the non-methane hydrocarbons ethane and propane over the North Atlantic, *Elem. Sci. Anth.*, 3, 000054, doi:10.12952/journal.elementa.000054, 2015.

Fo
Fo

785 Herzsprung, P., Hertkorn, N., Tümpeling, W., Harir, M., Friese, K. and Schmitt-Kopplin, P.: Understanding molecular formula assignment of Fourier transform ion cyclotron resonance mass spectrometry data of natural organic matter from a chemical point of view, *Anal. Bioanal. Chem.*, 406(30), 7977–7987, doi:10.1007/s00216-014-8249-y, 2014.

790 Hinks, M., Brady, M., Lignell, H., Song, M., Grayson, J., Bertram, A., Lin, P., Laskin, A., Laskin, J. and Nizkorodov, S.: Effect of viscosity on photodegradation rates in complex secondary organic aerosol materials, *Phys. Chem. Chem. Phys.*, 18(13), 8785–8793, doi:10.1039/c5cp05226b, 2015.

795 [Hoyle, C. R., Fuchs, C., Järvinen, E., Saathoff, H., Dias, A., Haddad, I. E., Gysel, M., Coburn, S. C., Tröstl, J., Bernhammer, A.-K., Bianchi, F., Breitenlechner, M., Corbin, J. C., Craven, J., Donahue, N. M., Duplissy, J., Ehrhart, S., Frege, C., Gordon, H., Höppel, N., Heinritzi, M., Kristensen, T. B., Molteni, U., Nichman, L., Pinterich, T., Prévôt, A. S. H., Simon, M., Slowik, J. G., Steiner, G., Tomé, A., Vogel, A. L., Volkamer, R., Wagner, A. C., Wagner, R., Wexler, A. S., Williamson, C., Winkler, P. M., Yan, C., Amorim, A., Dommen, J., Curtius, J., Gallagher, M. W., Flagan, R. C., Hansel, A., Kirkby, J., Kulmala, M., Möhler, O., Stratmann, F., Worsnop, D. R. and Baltensperger, U.: Aqueous phase oxidation of sulphur dioxide by ozone in cloud droplets, *Atmos. Chem. Phys.*, 16\(3\), 1693–1712, doi:10.5194/acp-16-1693-2016 , 2016.](#)

800 Huang, R., Zhang, Y., Bozzetti, C., Ho, K., Cao, J., Han, Y., Daellenbach, K. R., Slowik, J. G., Platt, S. M., Canonaco, F., Zotter, P., Wolf, R., Pieber, S. M., Bruns, E. A., Crippa, M., Ciarelli, G., Piazzalunga, A., Schwikowski, M., Abbaszade, G., Schnelle-Kreis, J., Zimmermann, R., An, Z., Szidat, S., Baltensperger, U., El Haddad, I. and Prevot, A. S. H.: High secondary aerosol contribution to particulate pollution during haze events in China, *Nature*, 514(7521), nature13774, doi:10.1038/nature13774, 2014.

805 Iinuma, Y., Boege, O., Graefe, R., and Herrmann, H.: Methyl-Nitrocatechols: Atmospheric Tracer Compounds for Biomass Burning Secondary Organic Aerosols, *Environ. Sci. Technol.*, 44, 8453–8459, doi:10.1021/es102938a, 2010.

810 Jimenez, J. L., Canagaratna, M. R., Donahue, N. M., Prevot, A. S. H., Zhang, Q., Kroll, J. H., DeCarlo, P. F., Allan, J. D., Coe, H., Ng, N. L., Aiken, A. C., Docherty, K. S., Ulbrich, I. M., Grieshop, A. P., Robinson, A. L., Duplissy, J., Smith, J. D., Wilson, K. R., Lanz, V. A., Hueglin, C., Sun, Y. L., Tian, J., Laaksonen, A., Raatikainen, T., Rautiainen, J., Vaattovaara, P., Ehn, M., Kulmala, M., Tomlinson, J. M., Collins, D. R., Cubison, M. J., Dunlea, E. J., Huffman, J. A., Onasch, T. B., Alfarra, M. R., Williams, P. I., Bower, K., Kondo, Y., Schneider, J., Drewnick, F., Borrmann, S., Weimer, S., Demerjian, K., Salcedo, D., Cottrell, L., Griffin, R., Takami, A., Miyoshi, T., Hatakeyama, S., Shimono, A., Sun, J. Y., Zhang, Y. M., Dzepina, K., Kimmel, J. R., Sueper, D., Jayne, J. T., Herndon, S. C., Trimborn, A. M., Williams, L. R., Wood, E. C., Middlebrook, A. M., Kolb, C. E., Baltensperger U. and Worsnop D. R.: Evolution of Organic Aerosols in the Atmosphere, *Science*, 326(5959), 1525–1529, doi:10.1126/science.1180353, 2009

815 Kaiser, J. W., Heil, A., Andreae, M. O., Benedetti, A., Chubarova, N., Jones, L., Morcrette, J.-J., Razinger, M., Schultz, M. G., Suttorp, M., and van der Werf, G. R.: Biomass burning emissions estimated with a global fire assimilation system based on observed fire radiative power, *Biogeosciences*, 9(1), 527–554, doi:10.5194/bg-9-527-2012, 2012.

820 Kido-Soule, M., Longnecker, K., Giovannoni, S. and Kujawinski, E.: Impact of instrument and experiment parameters on reproducibility of ultrahigh resolution ESI FT-ICR mass spectra of natural organic matter, *Org. Geochem.*, 41(8), 725–733, doi:10.1016/j.orggeochem.2010.05.017, 2010.

825 Kirpes, R. M., Bondy, A. L., Bonanno D., Moffet, R. C., Wang, B., Laskin, A., Ault, A. P., and Pratt, K. A.: Secondary Sulfate is Internally Mixed with Sea Spray Aerosol and Organic Aerosol in the Winter-Spring Arctic, *Atmos. Chem. Phys. Disc.*, 1–29, doi:10.5194/acp-2017-998, 2017.

Kleissl, J., Honrath, R. E., Dziobak, M. P., Tanner, D., Val Martín, M., Owen, R. C. and Helmig, D.: Occurrence of upslope flows at the Pico mountaintop observatory: A case study of orographic flows on a small, volcanic island, *J. Geophys. Res-Atmos.*, 112(D10), doi:10.1029/2006jd007565, 2007.

830 Koch, B. P. and Dittmar, T.: From mass to structure: an aromaticity index for high-resolution mass data of natural organic matter, *Rapid Commun. Mass Sp.*, 20(5), 926–932, doi:10.1002/rcm.2386, 2006

Koch, B. P. and Dittmar, T.: From mass to structure: an aromaticity index for high-resolution mass data of natural organic matter, *Rapid Commun. Mass Sp.*, 30(1), 250, doi: 10.1002/rcm.7433, 2016.

835 Koop, T., Bookhold, J., Shiraiwa, M. and Pöschl, U.: Glass transition and phase state of organic compounds: dependency on molecular properties and implications for secondary organic aerosols in the atmosphere, *Phys. Chem. Chem. Phys.*, 13(43), 19238–19255, doi:10.1039/c1cp22617g, 2011.

Kroll, J. H., Donahue, N. M., Jimenez, J. L., Kessler, S. H., Canagaratna, M. R., Wilson, K. R., Altieri, K. E., Mazzoleni, L. R., Wozniak, A. S., Bluhm, H., Mysak, E. R., Smith, J. D., Kolb, C. E. and Worsnop, D. R.: Carbon oxidation state as a metric for describing the chemistry of atmospheric organic aerosol, *Nat. Chem.*, 3(2), nchem.948, doi:10.1038/nchem.948, 2011.

[Lai, C., Liu, Y., Ma, J., Ma, Q. and He, H.: Degradation kinetics of levoglucosan initiated by hydroxyl radical under different environmental conditions, *Atmos. Environ.*, 91, 32–39, doi:10.1016/j.atmosenv.2014.03.054 , 2014.](#)

Laing, J. R., Jaffe, D. A., and Hee, J. R.: Physical and optical properties of aged biomass burning aerosol from wildfires in Siberia and the Western USA at the Mt. Bachelor Observatory, *Atmos. Chem. Phys.*, 16(23), 15185–15197, doi:10.5194/acp-16-15185-2016, 2016.

895 Lambe, A. T., Onasch, T. B., Massoli, P., Croasdale, D. R., Wright, J. P., Ahern, A. T., Williams, L. R., Worsnop, D. R., Brune, W. H., and Davidovits, P.: Laboratory studies of the chemical composition and cloud condensation nuclei (CCN) activity of secondary organic aerosol (SOA) and oxidized primary organic aerosol (OPOA), *Atmos. Chem. Phys.*, 11(17), 8913–8928, doi:10.5194/acp-11-8913-2011, 2011

900 Laskin, A., Laskin, J. and Nizkorodov, S.: Chemistry of Atmospheric Brown Carbon, *Chemical Reviews*, 115(10), 4335–4382, doi:10.1021/cr5006167, 2015

Lee, A. K. Y., Herckes, P., Leaitch, W. R., Macdonald, A. M. and Abbatt, J. P. D.: Aqueous OH oxidation of ambient organic aerosol and cloud water organics: Formation of highly oxidized products, *Geophys. Res. Lett.*, 38(11), n/a-n/a, doi:10.1029/2011gl047439, 2011.

905 Levin, E., McMeeking, G. R., Carrico, C. M., Mack, L. E., Kreidenweis, S. M., Wold, C. E., Moosmüller, H., Arnott, W. P., Hao, W. M., Collett, J. L. and Malm, W. C.: Biomass burning smoke aerosol properties measured during Fire Laboratory at Missoula Experiments (FLAME), *J. Geophys. Res.-Atmos.*, 115(D18), doi:10.1029/2009jd013601, 2010.

Li, Y., Pöschl, U. and Shiraiwa, M.: Molecular corridors and parameterizations of volatility in the chemical evolution of organic aerosols, *Atmos. Chem. Phys.*, 16(5), 3327–3344, doi:10.5194/acp-16-3327-2016, 2016.

910 Lignell, H., Hinks, M. and Nizkorodov, S.: Exploring matrix effects on photochemistry of organic aerosols, *P. Natl. Acad. Sci.*, 111(38), 13780–13785, doi:10.1073/pnas.1322106111, 2014.

[Lim, Y. B., Tan, Y., Perri, M. J., Seitzinger, S. P. and Turpin, B. J.: Aqueous chemistry and its role in secondary organic aerosol \(SOA\) formation, *Atmos. Chem. Phys.*, 10\(21\), 10521–10539, doi:10.5194/acp-10-10521-2010, 2010.](#)

915 Lin, P., Aiona, P. K., Li, Y., Shiraiwa, M., Laskin, J., Nizkorodov, S. A., and Laskin, A.: Molecular Characterization of Brown Carbon in Biomass Burning Aerosol Particles, *Environ. Sci. Technol.*, 50, 11815–11824, doi:10.1021/acs.est.6603024, 2016.

Liu, S. and Liang, X.: Observed Diurnal Cycle Climatology of Planetary Boundary Layer Height, *J. Climate*, 23(21), 5790–5809, doi:10.1175/2010jcli3552.1, 2010.

920 Liu, X., Huey, L. G., Yokelson, R. J., Selimovic, V., Simpson, I. J., Müller, M., Jimenez, J. L., Campuzano-Jost, P., Beyersdorf, A. J., Blake, D. R., Butterfield, Z., Choi, Y., Crounse, J. D., Day, D. A., Diskin, G. S., Dubey, M. K., Fortner, E., Hanisco, T. F., Hu, W., King, L. E., Kleinman, L., Meinardi, S., Mikoviny, T., Onasch, T. B., Palm, B. B., Peischl, J., Pollack, I. B., Ryerson, T. B., Sachse, G. W., Sedlacek, A. J., Shilling, J. E., Springston, S., Clair, J., Tanner, D. J., Teng, A. P., Wennberg, P. O., Wisthaler, A. and Wolfe, G. M.: Airborne measurements of western U.S. wildfire emissions: Comparison with prescribed burning and air quality implications, *J. Geophys. Res.-Atmos.*, 122(11), 6108–6129, doi:10.1002/2016jd026315, 2017.

925 Massoli, P., Lambe, A. T., Ahern, A. T., Williams, L. R., Ehn, M., Mikkilä, J., Canagaratna, M. R., Brune, W. H., Onasch, T. B., Jayne, J. T., Petäjä, T., Kulmala, M., Laaksonen, A., Kolb, C. E., Davidovits, P. and Worsnop, D. R.: Relationship between aerosol oxidation level and hygroscopic properties of laboratory generated secondary organic aerosol (SOA) particles, *Geophys. Res. Lett.*, 37(24), n/a-n/a, doi:10.1029/2010gl045258, 2010.

930 Mazzoleni, L. R., Ehrmann, B. M., Shen, X., Marshall, A. G. and Collett, J. L.: Water-Soluble Atmospheric Organic Matter in Fog: Exact Masses and Chemical Formula Identification by Ultrahigh-Resolution Fourier Transform Ion Cyclotron Resonance Mass Spectrometry, *Environ. Sci. Technol.*, 44(10), 3690–3697, doi:10.1021/es903409k, 2010.

Mazzoleni, L. R., Saranjampour, P., Dalbec, M. M., Samburova, V., Hallar, A. G., Zielinska, B., Lowenthal, D. H. and Kohl, S.: Identification of water-soluble organic carbon in non-urban aerosols using ultrahigh-resolution FT-ICR mass spectrometry: organic anions, *Environ. Chem.*, 9(3), 285–297, doi:10.1071/en11167, 2012.

935 Ng, N. L., Canagaratna, M. R., Jimenez, J. L., Chhabra, P. S., Seinfeld, J. H. and Worsnop, D. R.: Changes in organic aerosol composition with aging inferred from aerosol mass spectra, *Atmos. Chem. Phys.*, 11(13), 6465–6474, doi:10.5194/acp-11-6465-2011, 2011.

[Nguyen, T. V., Zhang, Q., Jimenez, J. L., Pike, M. and Carlton, A. G.: Liquid Water: Ubiquitous Contributor to Aerosol Mass, *Environ. Sci. Technol. Lett.*, 3\(7\), 257–263, doi:10.1021/acs.estlett.6b00167, 2016.](#)

940 O'Brien, R. E., Laskin, A., Laskin, J., Liu, S., Weber, R., Russell, L. M. and Goldstein, A. H.: Molecular characterization of organic aerosol using nanospray desorption/electrospray ionization mass spectrometry: CalNex 2010 field study, *Atmospheric Environment*, 68, 265–272, doi:10.1016/j.atmosenv.2012.11.056, 2013.

Olivier, J.G.J. and Berdowski, J.J.M.: Global emissions sources and sinks, in: *The Climate System*, Berdowski, J., Guicherit, R. and Heij, B.J., A.A. Balkema Publishers/Swets & Zeitlinger Publishers, Lisse, The Netherlands. 33-78, 2001.

945 Perraudin, E., Budzinski, H. and Villenave, E.: Kinetic Study of the Reactions of Ozone with Polycyclic Aromatic Hydrocarbons Adsorbed on Atmospheric Model Particles, *J. Atmos. Chem.*, 56(1), 57–82, doi:10.1007/s10874-006-9042-x, 2006.

950 Pfister, G. G., Emmons, L. K., Hess, P. G., Honrath, R. E., Lamarque, J. F., Val Martin, M., Owen, R. C., Avery, M. A., Browell, E. V., Holloway, J. S., Nedelev, P., Purvis, R., Ryerson, T. B., Sachse, G. W. and Schlager, H.: Ozone production from the 2004 North American boreal fires, *J. Geophys. Res.-Atmos.*, 111(D24), doi:10.1029/2006jd007695, 2006.

955 Pöschl, U.: Atmospheric Aerosols: Composition, Transformation, Climate and Health Effects, *Angew. Chem. Int. Edit.*, 44(46), 7520–7540, doi:10.1002/anie.200501122, 2005.

960 Putman, A. L., Offenberg, J. H., Fisseha, R., Kundu, S., Rahn, T. A. and Mazzoleni, L. R.: Ultrahigh-resolution FT-ICR mass spectrometry characterization of α -pinene ozonolysis SOA, *Atmos. Env.*, 46, 164–172, doi:10.1016/j.atmosenv.2011.10.003, 2012.

965 Quinn, P. K., Collins, D. B., Grassian, V. H., Prather, K. A., and Bates, T. S.: Chemistry and Related Properties of Freshly Emitted Sea Spray Aerosol, *Chem. Rev.*, 115(10), 4383–4399, doi:10.1021/cr500713g, 2015.

Rémillard, J., Kollias, P., Luke, E. and Wood, R.: Marine Boundary Layer Cloud Observations in the Azores, *J. Climate*, 25(21), 7381–7398, doi:10.1175/jcli-d-11-00610.1, 2012.

970 Schmitt-Kopplin, P., Gelencsér, A., Dabek-Zlotorzynska, E., Kiss, G., Hertkorn, N., Harir, M., Hong, Y. and Gebefügi, I.: Analysis of the Unresolved Organic Fraction in Atmospheric Aerosols with Ultrahigh-Resolution Mass Spectrometry and Nuclear Magnetic Resonance Spectroscopy: Organosulfates As Photochemical Smog Constituents, *Anal. Chem.*, 82(19), 8017–8026, doi:10.1021/ac101444r, 2010.

975 Schmitt-Kopplin, P., Liger-Belair, G., Koch, B., Flerus, R., Kattner, G., Harir, M., Kanawati, B., Lucio, M., Tziotis, D., Hertkorn, N. and Gebefügi, I.: Dissolved organic matter in sea spray: a transfer study from marine surface water to aerosols, *Biogeosciences*, 9(4), 1571–1582, doi:10.5194/bg-9-1571-2012, 2012.

980 Seibert, P. and Frank, A.: Source-receptor matrix calculation with a Lagrangian particle dispersion model in backward mode, *Atmos. Chem. Phys.*, 4, 51–63, <https://doi.org/10.5194/acp-4-51-2004>, 2004.

985 Shiraiwa, M., Ammann, M., Koop, T. and Pöschl, U.: Gas uptake and chemical aging of semisolid organic aerosol particles, *P. Natl. Acad. Sci.*, 108(27), 11003–11008, doi:10.1073/pnas.1103045108, 2011.

990 Slade, J. H. and Knopf, D. A.: Multiphase OH oxidation kinetics of organic aerosol: The role of particle phase state and relative humidity, *Geophys. Res. Lett.*, 41(14), 5297–5306, doi:10.1002/2014gl060582, 2014.

995 Shiraiwa, M., Li, Y., Tsimpidi, A., Karydis, V., Berkemeier, T., Pandis, S., Lelieveld, J., Koop, T. and Pöschl, U.: Global distribution of particle phase state in atmospheric secondary organic aerosols, *Nat. Commun.*, 8, ncomms15002, doi:10.1038/ncomms15002, 2017.

Shrivastava, M., Lou, S., Zelenyuk, A., Easter, R., Corley, R., Thrall, B., Rasch, P., Fast, J., Simonich, S., Shen, H. and Tao, S.: Global long-range transport and lung cancer risk from polycyclic aromatic hydrocarbons shielded by coatings of organic aerosol, *P. Natl. Acad. Sci.*, 114(6), 1246–1251, doi:10.1073/pnas.1618475114, 2017.

Sorooshian, A., Lu, M.-L., Brechtel, F., Jonsson, H., Feingold, G., Flagan, R. and Seinfeld, J.: On the Source of Organic Acid Aerosol Layers above Clouds, *Environ. Sci. Technol.*, 41(13), 4647–4654, doi:10.1021/es0630442, 2007.

Stohl, A., Forster, C., Frank, A., Seibert, P. and Wotawa, G.: Technical note: The Lagrangian particle dispersion model FLEXPART version 6.2, *Atmospheric Chemistry and Physics*, 5(9), 2461–2474, doi:10.5194/acp-5-2461-2005, 2005.

Tu, P., Hall, W. and Johnston, M.: Characterization of Highly Oxidized Molecules in Fresh and Aged Biogenic Secondary Organic Aerosol, *Anal. Chem.*, 88(8), 4495–4501, doi:10.1021/acs.analchem.6b00378, 2016.

U.S. Air Quality, Smog Blog. alg.umbc.edu, last access: 9 January 2018.

Vakkari, V., Kerminen, V., Beukes, J., Tiitta, P., Zyl, P., Josipovic, M., Venter, A., Jaars, K., Worsnop, D., Kulmala, M. and Laakso, L.: Rapid changes in biomass burning aerosols by atmospheric oxidation, *Geophys. Res. Lett.*, 41(7), 2644–2651, doi:10.1002/2014gl059396, 2014.

Val Martin, M., Honrath, R., Owen, R., Pfister, G., Fialho, P. and Barata, F.: Significant enhancements of nitrogen oxides, black carbon, and ozone in the North Atlantic lower free troposphere resulting from North American boreal wildfires, *J. Geophys. Res.-Atmos.*, 111(D23), n/a-n/a, doi:10.1029/2006jd007530, 2006.

Val Martin, M., Honrath, R., Owen, R. and Lapina, K.: Large-scale impacts of anthropogenic pollution and boreal wildfires on the nitrogen oxides over the central North Atlantic region, *J. Geophys. Res.-Atmos.*, 113(D17), doi:10.1029/2007jd009689, 2008a.

Val Martin, M., Honrath, R., Owen, R. and Li, Q.: Seasonal variation of nitrogen oxides in the central North Atlantic lower free troposphere, *J. Geophys. Res.-Atmos.*, 113(D17), doi:10.1029/2007jd009688, 2008b.

1000 Val Martin, M., Logan, J. A., Kahn, R. A., Leung, F.-Y., Nelson, D. L. and Diner, D. J.: Smoke injection heights from fires in North America: analysis of 5 years of satellite observations, *Atmos. Chem. Phys.*, 10(4), 1491–1510, doi:10.5194/acp-10-1491-2010, 2010.

1005 Virtanen, A., Joutsensaari, J., Koop, T., Kannisto, J., Yli-Pirilä, P., Leskinen, J., Mäkelä, J., Holopainen, J., Pöschl, U., Kulmala, M., Worsnop, D. and Laaksonen, A.: An amorphous solid state of biogenic secondary organic aerosol particles, *Nature*, 467(7317), nature09455, doi:10.1038/nature09455, 2010.

1010 [Vogel, A., Äijälä, M., Corrigan, A., Junninen, H., Ehn, M., Petäjä, T., Worsnop, D., Kulmala, M., Russell, L., Williams, J., and Hoffmann, T.: In situ submicron organic aerosol characterization at a boreal forest research station during HUMPPA-COPEC 2010 using soft and hard ionization mass spectrometry](#), *Atmos. Chem. Phys.*, 13(21), 10933–10950, doi:10.5194/acp-13-10933-2013, 2013.

1015 Volkamer, R., Jimenez, J. L., San Martini, F., Dzepina, K., Zhang, Q., Salcedo, D., Molina, L. T., Worsnop, D. R. and Molina, M. J.: Secondary organic aerosol formation from anthropogenic air pollution: Rapid and higher than expected, *Geophys. Res. Lett.*, 33(17), doi:10.1029/2006gl026899, 2006.

1020 [Volkamer, R., Ziemann, P. and Molina, M.: Secondary Organic Aerosol Formation from Acetylene \(C2H2\): seed effect on SOA yields due to organic photochemistry in the aerosol aqueous phase](#), *Atmos. Chem. Phys.*, 9(6), 1907–1928, doi:10.5194/acp-9-1907-2009, 2009.

1025 Walser, M. L., Desyaterik, Y., Laskin, J., Laskin, A. and Nizkorodov, S.: High-resolution mass spectrometric analysis of secondary organic aerosol produced by ozonation of limonene, *Phys. Chem. Chem. Phys.*, 10(7), 1009–1022, doi:10.1039/b712620d, 2007.

1030 [Warneke, P.: In-cloud chemistry opens pathway to the formation of oxalic acid in the marine atmosphere](#), *Atmos. Environ.*, 37(17), 2423–2427, doi:10.1016/s1352-2310(03)00136-5, 2003.

1035 Warneke, C., Bahreini, R., Brioude, J., Brock, C. A., Gouw, J., Fahey, D. W., Froyd, K. D., Holloway, J. S., Middlebrook, A., Miller, L., Montzka, S., Murphy, D. M., Peischl, J., Ryerson, T. B., Schwarz, J. P., Spackman, J. R. and Veres, P.: Biomass burning in Siberia and Kazakhstan as an important source for haze over the Alaskan Arctic in April 2008, *Geophys. Res. Lett.*, 36(2), n/a-n/a, doi:10.1029/2008gl036194, 2009.

1040 Wozniak, A. S., Willoughby, A. S., Gurganus, S. C. and Hatcher, P. G.: Distinguishing molecular characteristics of aerosol water soluble organic matter from the 2011 trans-North Atlantic US GEOTRACES cruise, *Atmos. Chem. Phys.*, 14(16), 8419–8434, doi:10.5194/acp-14-8419-2014, 2014.

1045 Ye, Q., Robinson, E. S., Ding, X., Ye, P., Sullivan, R. C. and Donahue, N. M.: Mixing of secondary organic aerosols versus relative humidity, *Proc. Natl. Acad. Sci.*, 113(45), 12649–12654, doi:10.1073/pnas.1604536113, 2016.

1050 Yu, J. Z., Huang, X., Xu, J. and Hu, M.: When Aerosol Sulfate Goes Up, So Does Oxalate: Implication for the Formation Mechanisms of Oxalate, *Environ. Sci. Technol.*, 39(1), 128–133, doi:10.1021/es049559f, 2005.

Zelenyuk, A., Imre, D. G., Wilson, J., Bell, D. M., Suski, K. J., Shrivastava, M., Beránek, J., Alexander, M. L., Kramer, A. L. and Massey-Simonich, S. L.: The effect of gas-phase polycyclic aromatic hydrocarbons on the formation and properties of biogenic secondary organic aerosol particles, *Faraday Discuss.*, 200, 143–164, doi:10.1039/c7fd00032d, 2017.

Zhang, B., Owen, R. C., Perlinger, J. A., Kumar, S., Wu, S., Val Martin, M., Kramer, L., Helmig, D. and Honrath, R. E.: A semi-Lagrangian view of ozone production tendency in North American outflow in the summers of 2009 and 2010, *Atmos. Chem. Phys.*, 14(5), 2267–2287, doi:10.5194/acp-14-2267-2014, 2014.

Zhang, B., Owen, R. C., Perlinger, J. A., Helmig, D., Val Martín, M., Kramer, L., Mazzoleni, L. R. and Mazzoleni, C.: Ten-year chemical signatures associated with long-range transport observed in the free troposphere over the central North Atlantic, *Elem. Sci. Anth.*, 5, doi:10.1525/elementa.194, 2017.

[Zhang, Q., Jimenez, J., Canagaratna, M., Allan, J., Coe, H., Ulbrich, I., Alfarra, M., Takami, A., Middlebrook, A., Sun, Y., Dzepina, K., Dunlea, E., Docherty, K., DeCarlo, P., Salcedo, D., Onasch, T., Jayne, J., Miyoshi, T., Shimono, A., Hatakeyama, S., Takegawa, N., Kondo, Y., Schneider, J., Drewnick, F., Borrmann, S., Weimer, S., Demerjian, K., Williams, P., Bower, K., Bahreini, R., Cottrell, L., Griffin, R., Rautiainen, J., Sun, J., Zhang, Y. and Worsnop, D.: Ubiquity and dominance of oxygenated species in organic aerosols in anthropogenically-influenced Northern Hemisphere midlatitudes](#), *Geophys. Res. Lett.*, 34(13), n/a-n/a, doi:10.1029/2007gl029979, 2007.

Zhao, Y., Hallar, A. G. and Mazzoleni, L. R.: Atmospheric organic matter in clouds: exact masses and molecular formula identification using ultrahigh-resolution FT-ICR mass spectrometry, *Atmos. Chem. Phys.*, 13(24), 12343–12362, doi:10.5194/acp-13-12343-2013, 2013.

Zobrist, B., Marcolli, C., Pedernera, D. and Koop, T.: Do atmospheric aerosols form glasses?, *Atmos. Chem. Phys.*, 8(17), 5221–5244, doi:10.5194/acp-8-5221-2008, 2008.

Tables

Table 1. Average concentrations ($\mu\text{g}/\text{m}^3$) of major ions and organic carbon.

Component	PMO-1	PMO-2	PMO-3
Acetate	0.0519 \pm 0.0001	0.004587 \pm 0.000005	0.0071 \pm 0.0002
Formate	0.0289 \pm 0.0003	0.00438 \pm 0.00007	0.0119 \pm 0.0001
MSA	0	0.00439 \pm 0.00006	0.00232 \pm 0.00002
Chloride	0.0104 \pm 0.0003	0	0.0310 \pm 0.0001
Nitrate	0.189 \pm 0.002	0.0173 \pm 0.0004	0.3010 \pm 0.00028
Sulfate	0.338 \pm 0.004	1.07 \pm 0.01	0.421 \pm 0.003
Oxalate	0.0938 \pm 0.00070	0.0897 \pm 0.00181	0.05222 \pm 0.00002
Sodium	0.2101 \pm 0.0004*	0.2560 \pm 0.0001*	0.548 \pm 0.005*
Ammonium	0.1364 \pm 0.0004	0.2394 \pm 0.00001	0.1193 \pm 0.00062
Potassium	0.0791 \pm 0.0020**	0.0126 \pm 0.0002	0.0197 \pm 0.0003
OC	2.07 \pm 0.02	0.478 \pm 0.026	0.87 \pm 0.10

1055 *Sodium concentrations were not background subtracted due to inconsistent and high blank levels, they are included to provide an upper limit on the approximate sodium concentrations.

1060 **Replicate measurements of potassium were inconsistent. The sample could not be re-analyzed because there was no remaining sample. Standard deviation was determined by looking at the average standard deviation of 36 potassium measurements in other samples. This sample should only be considered as elevated potassium and only minimal importance placed on the actual measured value.

1065

1070 **Table 2.** Molecular formula composition with abundance weighted average values and the numbers of formulas for each elemental group.

Sample	Group	O/C _w	H/C _w	DBE _w	OS _{Cw}	Number
PMO-1	All	0.48 \pm 0.13	1.30 \pm 0.28	7.74 \pm 3.38	-0.42 \pm 0.43	3168
PMO-2	All	0.57 \pm 0.17	1.36 \pm 0.22	6.42 \pm 2.54	-0.30 \pm 0.46	2121
PMO-3	All	0.45 \pm 0.11	1.34 \pm 0.41	7.45 \pm 3.15	-0.50 \pm 0.41	1820
PMO-1	CHO	0.47 \pm 0.14	1.31 \pm 0.29	7.43 \pm 3.68	-0.37 \pm 0.44	1848
PMO-2	CHO	0.55 \pm 0.17	1.35 \pm 0.25	6.43 \pm 3.66	-0.26 \pm 0.45	1281
PMO-3	CHO	0.44 \pm 0.14	1.37 \pm 0.31	6.93 \pm 3.82	-0.48 \pm 0.48	1183
PMO-1	CHNO	0.49 \pm 0.15	1.2 \pm 0.26	9.44 \pm 3.09	-0.50 \pm 0.3	1120
PMO-2	CHNO	0.59 \pm 0.14	1.25 \pm 0.19	8.20 \pm 2.19	-0.38 \pm 0.29	561
PMO-3	CHNO	0.49 \pm 0.14	1.23 \pm 0.21	9.25 \pm 2.41	-0.52 \pm 0.25	608
PMO-1	CHOS	0.48 \pm 0.14	1.78 \pm 0.35	2.87 \pm 3.28	-1.20 \pm 0.42	200
PMO-2	CHOS	0.74 \pm 0.34	1.57 \pm 0.23	4.05 \pm 2.45	-0.54 \pm 0.51	274
PMO-3	CHOS	0.40 \pm 0.14	1.90 \pm 0.47	1.60 \pm 4.29	-1.50 \pm 0.20	29

1075

Figures

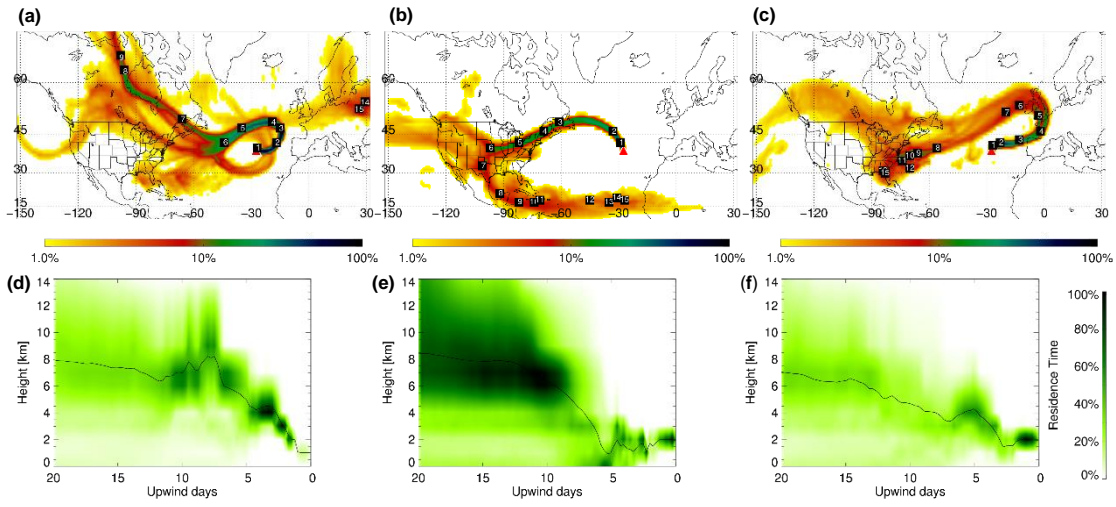


Figure 1. FLEXPART retroplumes for 28 June 2013 06:00 (PMO-1, (a, d)), 6 July 2014 03:00 (PMO-2, (b, e)), and 21 June 03:00 2015 (PMO-3, (c, f)): column integrated residence time over the 20-day transport time (a-c) and vertical distribution of the retroplume residence time at given upwind times (d-f). The labels indicate the approximate locations of the center of the plume for each of the transport days. Residence time is color coded by logarithmic grades representing its ratio to the location of maximal integrated residence time (100%). The black line in d-f indicates the mean height of the plume during transport.

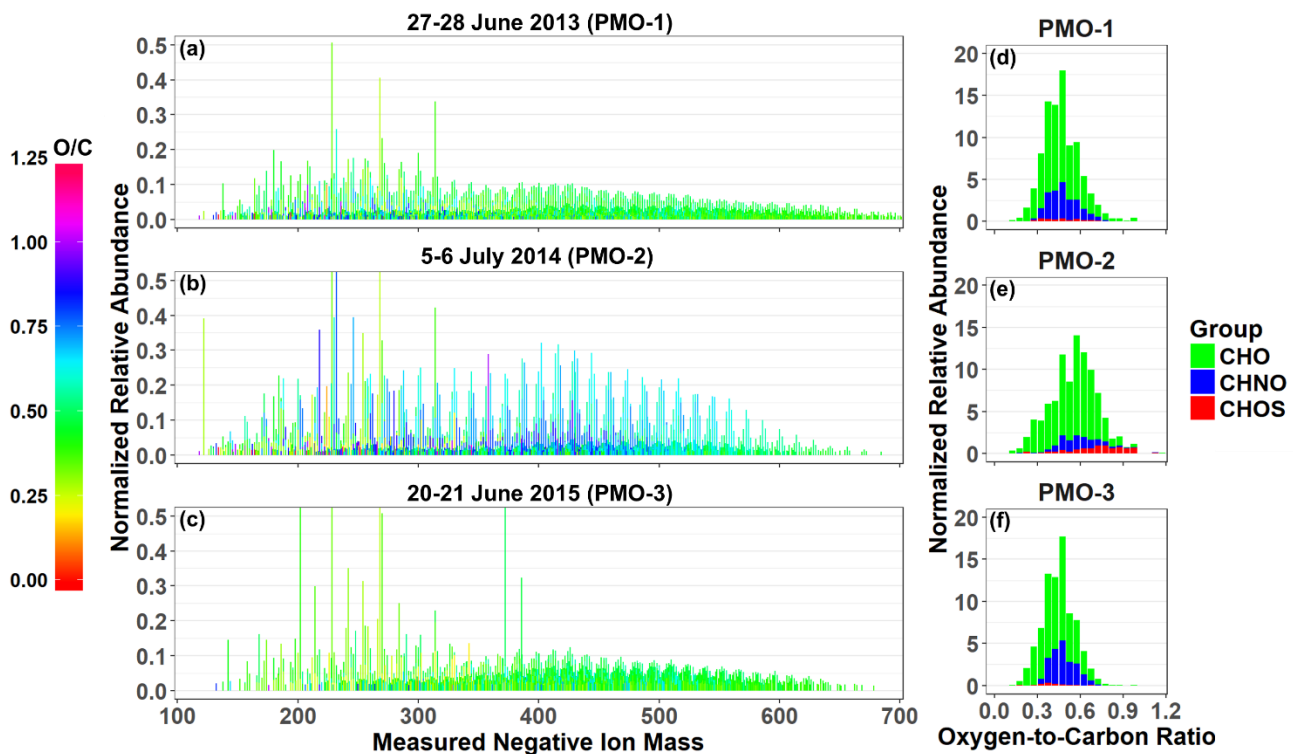


Figure 2. Reconstructed negative ion mass spectra (a-c) and O/C histograms (d-f) for the three PMO samples. The color in the mass spectra indicates the O/C value for the molecular formula it represents. The tallest peaks in the mass spectra exceed the range, this was done to improve the visibility of the lower abundance species (see also Fig. S6).

1100

1105

1110

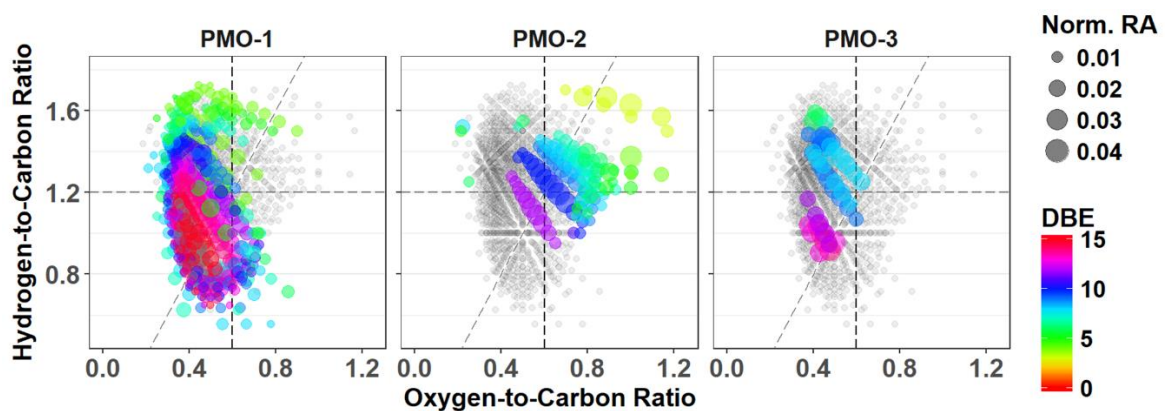


Figure 3. Van Krevelen plots for the CHNO species with all identified CHNO species (grey) and unique species (colored). The color represents the number of double bond equivalents in the corresponding molecular formula. The diagonal line is an oxidation line ($OS_C = 0$ for C, H, O elements; Tu et al., 2016), where the more oxidized formulas are on the right side and less oxidized are on the left.

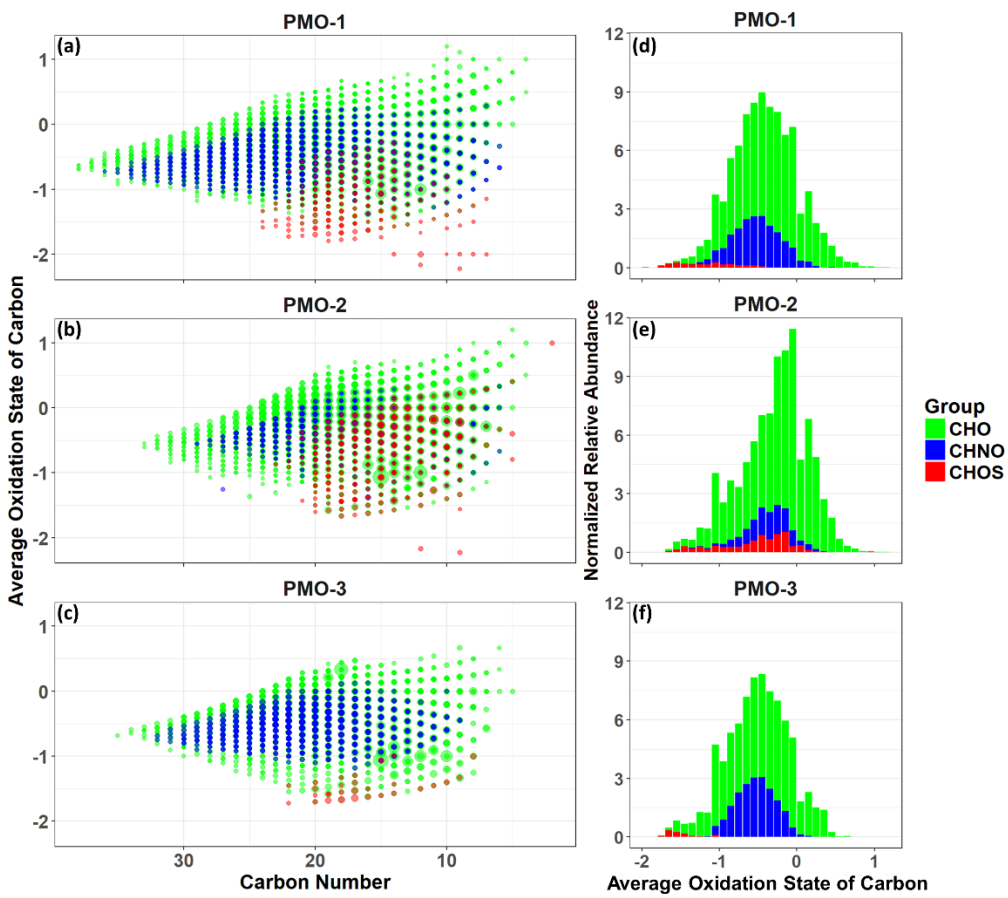
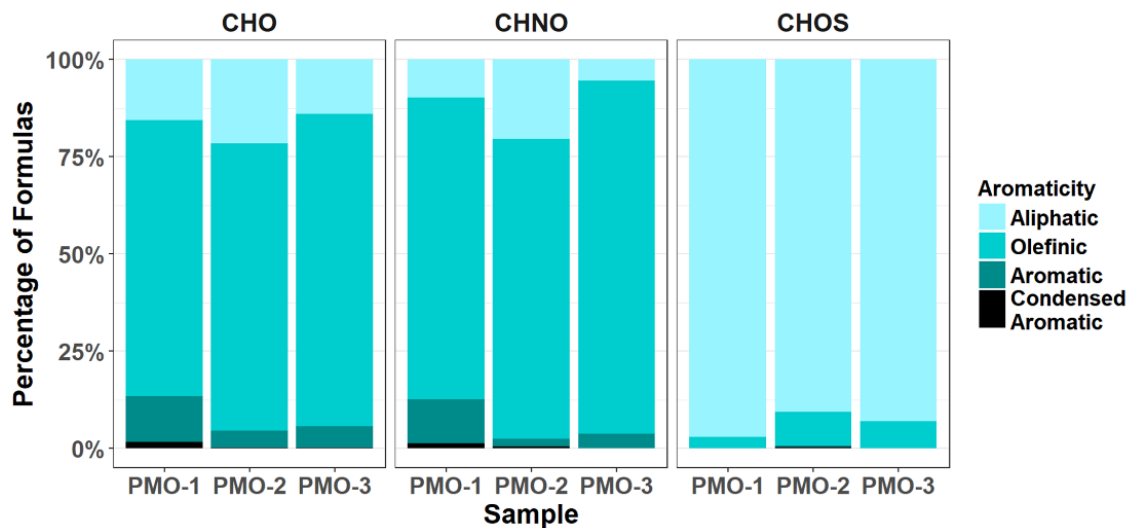


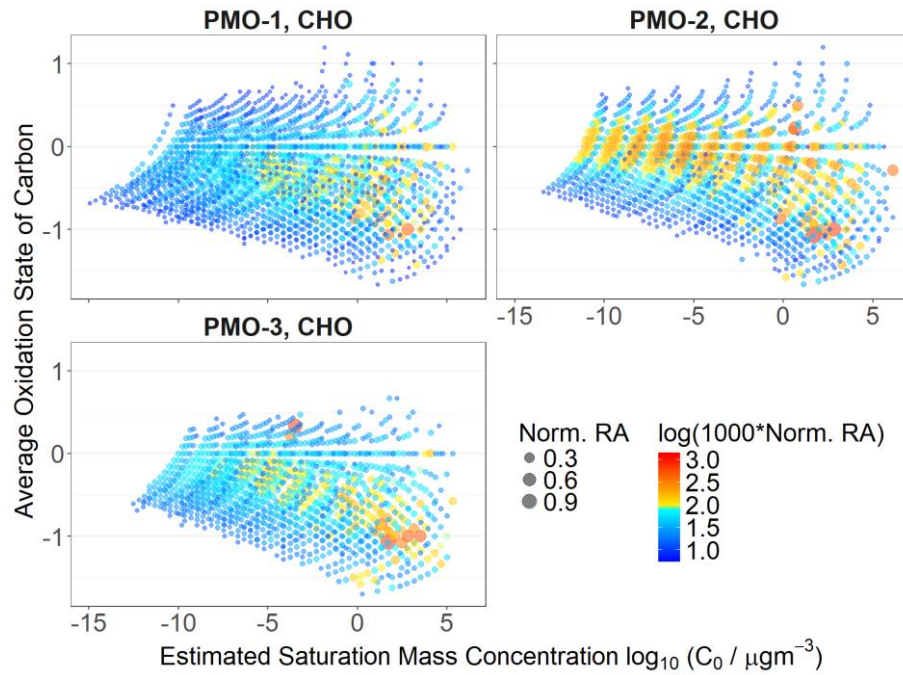
Figure 4. Average OS_C vs. carbon number plots for molecular formula identified in each of PMO samples (a-c). The size of the symbols is scaled to the analyte relative abundance and the color represents the elemental group: CHO (green), CHNO (blue), and CHOS (red). The right panel (d-f) contains average OS_C histograms based on the sum of normalized abundance.

1125

1130



1135 **Figure 5.** Normalized bar charts for the aromaticity of the three PMO samples, calculated using the Koch and Dittmar (2006; 2016) modified aromaticity index (AI_{mod}).



1140 **Figure 6.** OS_C vs. volatility estimated using the Li et al. (2016) method for the CHO species in the three samples. The size is
determined by the normalized relative abundance and the color is determined by the logarithm of the normalized relative
abundance multiplied by 1000.

1145

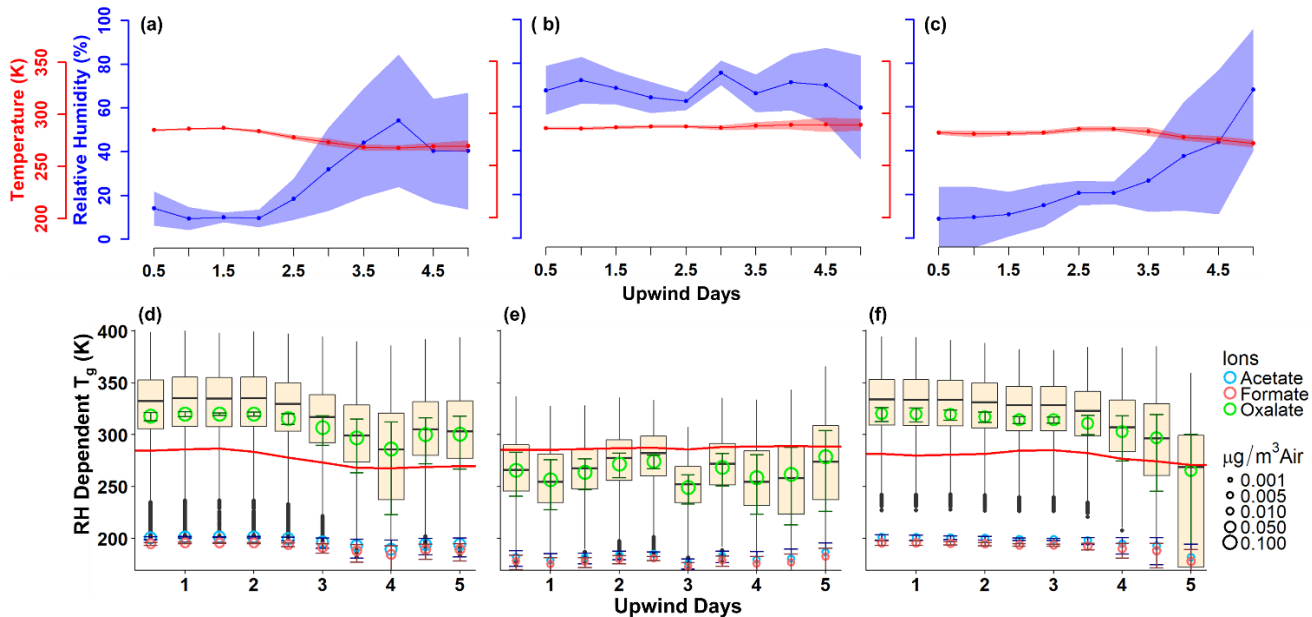


Figure 7. Panels a-c contain the ambient conditions extracted from the GFS analysis along the FLEXPART modeled path weighted by the residence time for PMO-1, PMO-2, and PMO-3, respectively. The line represents the mean value and the shading represents one standard deviation of values. Panels d-f contain the boxplot distributions of the relative humidity dependent T_g values for molecular formulas using the maximum, mean, and minimum RH for PMO-1, PMO-2, and PMO-3, respectively. The T_g values for the full composition of each sample were calculated using the maximum, mean, and minimum RH and then all three sets of data are combined and plotted as a single distribution for each time period. The open circles represent the abundance and Boyer-Kauzmann estimated T_g for the acid forms of the three most abundant low MW organic ions, the bars around the circles represent the range of possible T_g values for those compounds when the range of RH is considered. The red line demonstrates the ambient temperature at each time point, as extracted from GFS. The centerline of the boxplot represents the median, the top and bottom of the “box” represent the third and first quartiles, respectively. The “whiskers” represent $Q3 + 1.5 \times \text{IQR}$ (maximum), and $Q1 - 1.5 \times \text{IQR}$ (minimum).

1150

1155

1160

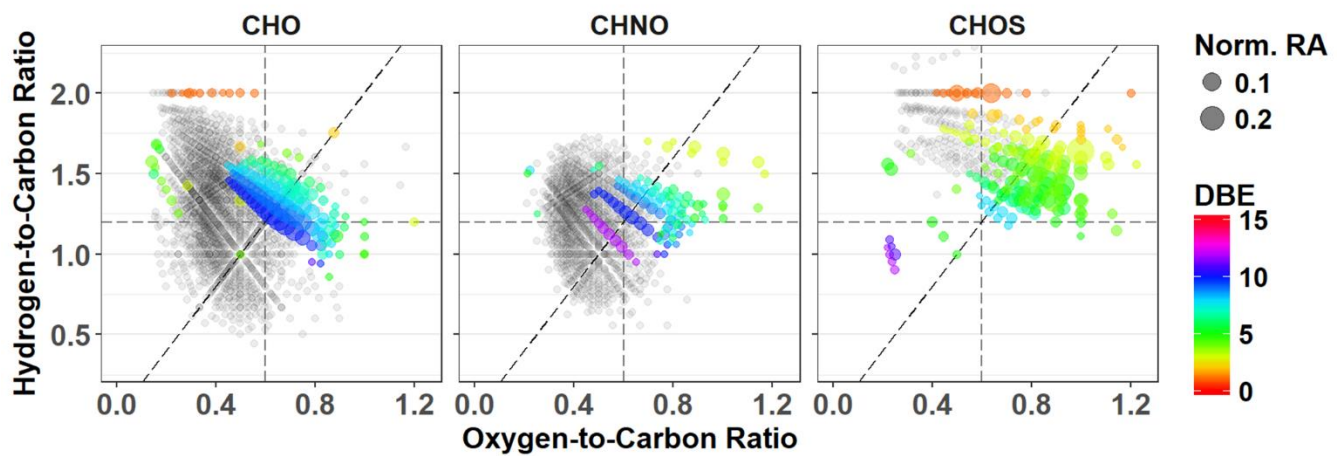


Figure 8. PMO-2 van Krevelen plots for unique molecular formulas separated by group. Symbols are scaled to indicate the normalized relative abundance. The DBE is indicated for each of unique molecular formulas using colored symbols. Formulas common with other samples are provided in grey for context.

1165